



**HAL**  
open science

## The temporal evolution of the carbon isotope composition of calcite in the presence of cyanobacteria

Christian Grimm, Vasileios Mavromatis, Albrecht Leis, Oleg S Pokrovsky,  
Eric H Oelkers

### ► To cite this version:

Christian Grimm, Vasileios Mavromatis, Albrecht Leis, Oleg S Pokrovsky, Eric H Oelkers. The temporal evolution of the carbon isotope composition of calcite in the presence of cyanobacteria. *Chemical Geology*, 2021, 584, pp.120556. 10.1016/j.chemgeo.2021.120556 . hal-03384297

**HAL Id: hal-03384297**

**<https://hal.science/hal-03384297v1>**

Submitted on 18 Oct 2021

**HAL** is a multi-disciplinary open access archive for the deposit and dissemination of scientific research documents, whether they are published or not. The documents may come from teaching and research institutions in France or abroad, or from public or private research centers.

L'archive ouverte pluridisciplinaire **HAL**, est destinée au dépôt et à la diffusion de documents scientifiques de niveau recherche, publiés ou non, émanant des établissements d'enseignement et de recherche français ou étrangers, des laboratoires publics ou privés.

# The temporal evolution of the carbon isotope composition of calcite in the presence of cyanobacteria

Christian Grimm<sup>1,\*</sup>, Vasileios Mavromatis (Βασίλειος Μαυρομάτης)<sup>1</sup>, Albrecht Leis<sup>2</sup>, Oleg S. Pokrovsky<sup>1,3</sup>, Eric H. Oelkers<sup>1\*</sup>

<sup>1</sup> Géosciences Environnement Toulouse, CNRS-UPS-OMP, 14 av. Édouard Belin, 31400 Toulouse, France.

<sup>2</sup> R-AquaConSol GmbH, Steyrergasse 21, 8010 Graz, Austria.

<sup>3</sup> BIO-GEO-CLIM Laboratory, Tomsk State University, 36 Lenina Prospekt, Tomsk, 630050, Russia

\* Corresponding authors

## Abstract

Quantifying the link between cyanobacterial activity and the carbon isotope signature of precipitated carbonate minerals is crucial for reconstructing the environmental conditions present at the time of carbonate mineral formation. In this study, calcite was precipitated in the presence and absence of *Synechococcus* sp. cyanobacteria in batch reactors. The temporal evolution of the carbon isotope composition of calcite ( $\delta^{13}\text{C}_{\text{Calcite}}$ ) and dissolved inorganic carbon ( $\delta^{13}\text{C}_{\text{DIC}}$ ) was monitored to evaluate the rate and degree to which the carbon isotope compositions in calcite are modified during and after its precipitation. The presence of cyanobacteria promoted calcium carbonate formation by increasing fluid pH and the  $\text{CaCO}_3$  saturation state. It also changed significantly the carbon isotope composition of dissolved inorganic carbon due to the preferential incorporation of  $^{12}\text{C}$  into the biomass. This generated an isotope disequilibrium between the calcite and the aqueous fluid phase over time after the

calcite precipitated. The carbon isotope composition of the calcite evolved continuously towards mineral-fluid isotope equilibrium after its precipitation, at geometric surface area normalized rates ranging from  $1.75 \times 10^{-14}$  to  $1.71 \times 10^{-13}$  mol  $^{13}\text{C}/\text{m}^2/\text{s}$ . These rates are sufficiently fast such that the  $\delta^{13}\text{C}_{\text{DIC}}$  value of aqueous fluids in calcite-rich rocks would be buffered by the  $\delta^{13}\text{C}_{\text{Calcite}}$  value of the co-existing calcite. Mass balance calculations suggest that the carbon isotope composition of calcite could change noticeably when the calcite is in isotope disequilibrium with its co-existing fluid, for example through the presence of a local  $^{12}\text{C}$  sink such as photosynthetic microorganisms or  $^{12}\text{C}$  source such as decomposition of organic material.

## **Keywords**

Carbon isotopes, calcite, cyanobacteria, isotope re-equilibration

## **1. INTRODUCTION**

The precipitation of carbonate minerals is a fundamental process in the Earth's carbon cycle (e.g., Archer and Maier-Reimer, 1994; Berner et al., 1983; Berner, 1992, 2004). The isotope compositions of carbonate minerals are assumed to reflect the conditions prevailing during their precipitation (e.g., Broecker, 1970; Epstein et al., 1953; Kump and Arthur, 1999; McCrea, 1950; McDermott, 2004; Schidlowski and Junge, 1981; Urey et al., 1951). As such, these compositions have become a widespread tool to reconstruct the environmental conditions present at the time of carbonate mineral formation. For example, the carbon isotope compositions of calcite and dolomite have been used to provide insight into past carbon cycling (Assayag et al., 2008; Bartley and Kah, 2004; Hayes et al., 1999) and to trace the link between biological activity and the rise of atmospheric oxygen in the Precambrian (e.g., Botz et al.,

1996; Broecker, 1970; Schrag et al., 2013; Whiticar, 1999). Organic carbon exhibits distinct carbon isotope compositions due to the preferential uptake of  $^{12}\text{C}$  during photosynthesis (Johnston and Fischer, 2012; O'Leary, 1988). Thus, at times of high primary productivity and organic carbon burial, carbon isotope compositions in the atmosphere, in dissolved inorganic carbon, and in precipitated carbonate minerals are enriched in the  $^{13}\text{C}$  isotope. Consequently, the  $\delta^{13}\text{C}$  values of carbonate minerals in the geological record to interpret past environmental conditions. The successful application of this environmental proxy however, requires that these isotope signatures be preserved over vast timescales.

The degree to which the isotope compositions of carbonate minerals can be preserved over geological timescales is a critical question for the estimation of paleo-environmental conditions. Numerous studies have reported the modification of mineral isotope compositions during diagenesis (e.g., Dickson and Coleman, 1980; Banner and Hanson, 1990; Brand and Veizer, 1980, 1981; Swart, 2015; Gorski and Fantle, 2017). This natural process has been attributed to coupled dissolution-precipitation at the mineral-fluid interface, and the degree of isotope exchange depends on the isotope disequilibrium between the mineral and the fluid phase (Brand and Veizer, 1980, 1981). Field (Eichinger, 1983) and laboratory (Mozeto et al., 1984; Wendt, 1971; Pederson et al., 2019) evidence affirms that carbon isotope exchange between fluids and carbon bearing phases is a widespread process that needs to be taken into account to accurately determine the  $^{14}\text{C}$  ages of groundwaters (Gonfiantini and Zuppi, 2003; Han et al., 2014; Han and Plummer, 2013). Such observations raise the question of how well carbonate minerals preserve their isotope compositions over long timescales and how well these compositions record their penecontemporaneous depositional environment.

One of the drivers of carbon mineral-fluid isotope disequilibria in natural systems stems from bacterial activity. The presence of cyanobacteria effects the carbon isotope compositions of dissolved inorganic carbon and of the precipitating carbonates through their metabolic

activity, which preferentially uptake  $^{12}\text{C}$  during photosynthesis (e.g., Ferris et al., 1997; Andres et al., 2006; Power et al., 2011; Brady et al., 2013; Mavromatis et al., 2015). Other studies have shown that cyanobacteria can promote carbonate mineral precipitation by increasing solution pH and the degree of  $\text{CaCO}_3$  supersaturation during photosynthesis (Merz, 1992; Riding, 2006). As such, bacterial activity exerts a major control on the carbon isotope composition of dissolved inorganic carbon (DIC) in natural waters, which in turn influences the isotope composition of carbonates precipitated at or near to isotope equilibrium with these fluids.

The present study was motivated by that of Mavromatis et al. (2015), who studied the re-equilibration of the carbon isotope signatures of precipitated hydrous Mg-carbonates in contact with an aqueous fluid containing growing cyanobacteria. The presence of cyanobacteria caused the rapid precipitation of the hydrous Mg-carbonates. Following this precipitation, the isotope composition of DIC in the aqueous phase evolved dramatically over time. It was found that the carbon isotope composition of the hydrous Mg-carbonates evolved continuously after its precipitation and remained close to isotope equilibrium with the DIC for the remainder of 30-day long experiments despite no measurable change in its mass. The present study was initiated to assess if a similar rapid carbon isotope exchange could be observed between calcite and the aqueous fluid in the absence of net mineral dissolution or precipitation.

A significant number of recent studies have also reported substantial isotope exchange between carbonate minerals and their co-existing fluids in the absence of net mineral dissolution or precipitation. For example, Mavromatis et al. (2016) reported a rapid equilibration of Ba isotopes in witherite in contact with an aqueous fluid after fluid-mineral chemical equilibrium was attained. Oelkers et al. (2019) reported the rapid resetting of the Ca isotope compositions of calcite in aqueous solutions that were in chemical equilibrium, but isotope disequilibrium with the mineral. The rapid alteration of the calcium isotope compositions of foraminiferal test at ambient temperatures at near to bulk equilibrium conditions, but in the presence of

isotopically distinct fluids, was reported by Chanda et al. (2019). The change in isotope composition of minerals at bulk chemical equilibrium is also the basis for determining experimentally equilibrium isotope fractionation factors using the three-isotope method (e.g., Beard et al., 2010; Li et al., 2011; Frierdich et al., 2014; Stamm et al., 2019, 2020).

In this study we conducted a series of batch calcite precipitation experiments in the presence of *Synechococcus* sp. cyanobacterium and monitored the temporal evolution of the carbon isotope composition in the fluid and solid phases. These observations were applied to assess the rate and degree to which stable carbon isotope compositions in calcite could be modified due to fluid-mineral isotope disequilibrium at near to bulk equilibrium conditions. The purpose of this paper is to report the results of this experimental study and to use these results to assess the degree to which calcite carbon isotope signatures might be changed over time in natural systems.

## 2. THEORETICAL CONSIDERATIONS

Carbon isotope compositions in this paper are presented in the delta notation given by:

$$\delta^{13}\text{C}_{\text{Sample}} (\text{‰}) = 10^3 \cdot \left( \frac{{}^{13/12}\text{C}_{\text{Sample}}}{{}^{13/12}\text{C}_{V\text{-}PDB}} - 1 \right), \quad (1)$$

where  ${}^{13/12}\text{C}$  refers to the indicated molar  ${}^{13}\text{C}$  to  ${}^{12}\text{C}$  isotope ratio,  $\delta^{13}\text{C}$  provides the normalized value of this ratio, and the subscripts Sample and *V-PDB* represent the sample of interest and the *V-PDB* international standard, respectively. Note that all calcite  $\delta^{13}\text{C}$  values ( $\delta^{13}\text{C}_{\text{Calcite}}$ ) reported in this study refer to the average bulk isotope composition of this solid.

In this study, calcite was precipitated from aqueous carbonate solutions in the presence of cyanobacteria and in contact with the atmosphere. In such systems there are several processes

that affect the carbon isotope composition of dissolved inorganic carbon ( $\delta^{13}\text{C}_{\text{DIC}}$ ) as summarized in Fig. 1. The  $\delta^{13}\text{C}_{\text{DIC}}$  values in these experiments are initially controlled by the carbon isotope composition of the carbonate and bicarbonate powder added to water to produce the initial reactive fluids. This value is subsequently influenced by 1) carbon exchange with the atmospheric  $\text{CO}_2$  that was continuously bubbled in the reactors, 2) photosynthetic uptake of DIC by growing cyanobacteria, 3) live cell respiration and dead cell lysis together with the subsequent heterotrophic degradation of organic compounds to dissolved carbon species, and 4) DIC removal from the fluid by calcite precipitation. These processes are described in detail in the following section.

### 2.1 Equilibrium fractionation between atmospheric $\text{CO}_2$ and DIC

An estimate of  $\delta^{13}\text{C}_{\text{DIC}}$  values in equilibrium with the atmosphere can be made by taking account of the distinct equilibrium fractionation factors of each major carbon species present in the aqueous fluids using (Myrntinen et al., 2012):

$$\delta^{13}\text{C}_{\text{DIC}} = \sum_i \left( x_i \cdot \left( \delta^{13}\text{C}_{\text{CO}_2} + 10^3 \ln \alpha^{13}\text{C}_{i-\text{CO}_2(\text{g})} \right) \right), \quad (2)$$

where  $x_i$  designates the mole fraction of the  $i$ th aqueous carbon species and  $\delta^{13}\text{C}_{\text{CO}_2}$  designates the carbon isotope composition of atmospheric  $\text{CO}_2$ , which was taken from Mavromatis et al. (2015), who conducted experiments in the same laboratory ( $\delta^{13}\text{C}_{\text{CO}_2} = -8.5 \pm 1\%$ ). The term  $10^3 \ln \alpha^{13}\text{C}_{i-\text{CO}_2(\text{g})}$  refers to the equilibrium fractionation factor between the  $i$ -th aqueous carbon species and  $\text{CO}_2(\text{g})$ . Note that as the equilibrium fractionation factor for each aqueous carbon species is distinct, the  $\delta^{13}\text{C}_{\text{DIC}}$  value in equilibrium with the atmosphere is a function of aqueous fluid pH and composition. This variation of fractionation factors with pH has led to discrepancies in aqueous  $\text{CO}_2$ - $\text{CO}_2(\text{g})$  equilibrium isotope fractionation factors reported in the literature (see Myrntinen et al., 2012). The fractionation factors  $10^3 \ln \alpha^{13}\text{C}_{\text{HCO}_3^- - \text{CO}_2(\text{g})} = 7.93$

and  $10^3 \ln \alpha^{13}\text{C}_{\text{CO}_3^{2-}-\text{CO}_2(\text{g})} = 5.92$  adopted in this study for 25°C were taken from Zhang et al. (1995). These fractionation factors indicate that  $\delta^{13}\text{C}_{\text{DIC}}$  values in equilibrium with atmospheric  $\text{CO}_2$  become more depleted in  $^{13}\text{C}$  with increasing pH at  $\text{pH} > 7$ . Note in the present study the only the  $\text{HCO}_3^-$  and  $\text{CO}_3^{2-}$  aqueous species were taken into account in the estimation of gas-DIC equilibrium carbon isotope fractionation factors owing to the lack of precise fractionation factors for other potentially forming DIC bearing species.

## 2.2 Carbon degassing

The effect of carbon degassing to the atmosphere can be quantified using a modified Rayleigh equation (Wynn et al., 2005):

$$\delta^{13}\text{C}_{\text{DIC}} = \left( 10^3 \cdot \left( F^{(\alpha^{13}\text{C}_{\text{DIC}-\text{CO}_2(\text{g})} - 1)} - 1 \right) \right) + \delta^{13}\text{C}_{\text{initial}} \cdot F^{(\alpha^{13}\text{C}_{\text{DIC}-\text{CO}_2(\text{g})} - 1)}. \quad (3)$$

Equation (3) allows calculation of the dissolved inorganic carbon isotope composition of the aqueous fluid,  $\delta^{13}\text{C}_{\text{DIC}}$ , after the fraction  $(1 - F)$  of carbon has been removed from the DIC pool by degassing. The initial carbon isotope signature of the aqueous fluid is given by  $\delta^{13}\text{C}_{\text{initial}}$ . The term  $\alpha^{13}\text{C}_{\text{DIC}-\text{CO}_2(\text{g})}$  designates the  $\text{DIC} - \text{CO}_2(\text{g})$  equilibrium isotope fractionation factor, which will vary during degassing due to fluid pH changes and its influence on the aqueous speciation of DIC. This effect can be calculated taking account of the carbon species present in the aqueous fluid using (Zhang et al., 1995):

$$10^3 \ln \alpha^{13}\text{C}_{\text{DIC}-\text{CO}_2(\text{g})} = \sum_i (x_i \cdot 10^3 \ln \alpha^{13}\text{C}_{i-\text{CO}_2(\text{g})}), \quad (4)$$

where  $10^3 \ln \alpha^{13}\text{C}_{i-\text{CO}_2(\text{g})}$  again refers to the equilibrium fractionation factor between the  $i$ th aqueous species and  $\text{CO}_2(\text{g})$  and  $x_i$  to the mole fraction of the subscripted aqueous carbon species present in the aqueous solution.

### 2.3 Effect of cyanobacteria on $\delta^{13}\text{C}_{\text{DIC}}$

Biomass produced during photosynthesis preferentially consumes  $^{12}\text{C}$  thus increasing  $\delta^{13}\text{C}_{\text{DIC}}$  values (see Fig. 1 and O'Leary, 1988; Johnston and Fischer, 2012). This has been observed in numerous natural and experimental studies (e.g., Ferris et al., 1997; Andres et al., 2006; Power et al., 2011; Brady et al., 2013; Mavromatis et al., 2015). Cyanobacteria may also release carbon relatively rich in  $^{12}\text{C}$  to the aqueous fluid during cell lysis and death. If respiration predominates over photosynthesis, as is common in many natural environments, (Schulte et al., 2011) this combined process will lower  $\delta^{13}\text{C}_{\text{DIC}}$  values of the aqueous fluid.

### 2.4 Calcium carbonate precipitation

The offset of  $\delta^{13}\text{C}$  values between calcite and DIC can be expressed by a fractionation factor ( $\Delta^{13}\text{C}_{\text{Calcite-DIC}}$ ) given by:

$$\Delta^{13}\text{C}_{\text{Calcite-DIC}} = \delta^{13}\text{C}_{\text{Calcite}} - \delta^{13}\text{C}_{\text{DIC}}. \quad (5)$$

As is the case for the equilibrium fractionation factors between atmospheric  $\text{CO}_2$  and DIC, the value of  $\Delta^{13}\text{C}_{\text{Calcite-DIC}}$  depends on the aqueous speciation. At isotope equilibrium,  $25^\circ\text{C}$ , and in aqueous fluids where dissolved carbon is dominated by the  $\text{HCO}_3^-$  species,  $\Delta^{13}\text{C}_{\text{Calcite-DIC}}$  has been reported to range between  $+0.83 \text{‰}$  and  $+1.96 \text{‰}$  (Deines et al., 1974; Jimenez-Lopez et al., 2006; Polag et al., 2010; Romanek et al., 1992), consistent with the preferential incorporation of  $^{13}\text{C}$  into calcite compared to its co-existing aqueous fluid. The formation of aqueous carbonate species other than  $\text{HCO}_3^-$  will influence this equilibrium fractionation factor. For example, at  $\text{pH} > 9$ , the equilibrium value  $\Delta^{13}\text{C}_{\text{Calcite-DIC}}$  will increase with pH due to the formation of the aqueous  $\text{CO}_3^{2-}$  species.

### 3. METHODS

#### 3.1 *Microcosm precipitation experiments*

The experimental protocol adopted in this study is similar to that used by Mavromatis et al., (2012; 2015). Calcite precipitation was performed in sterile 1000 ml borosilicate glass reactors containing Sigma-Aldrich C3061 BG-11 growth medium. The initial aqueous fluid compositions of each experiment are provided in Table 1 and were chosen to promote sufficient calcium carbonate precipitation to produce adequate calcite and dissolved carbonate concentrations for chemical and isotope analyses, but avoiding unfavorable growth conditions for the cyanobacteria. The supersaturation of these initial fluids with respect to calcite ( $1.8 \leq SI_{\text{Calcite}} \leq 3.0$ ; where  $SI_{\text{Calcite}}$  refers to the saturation index of the fluid with respect to calcite<sup>1</sup>) ensured its rapid homogeneous precipitation. All initial reactive fluids were either autoclaved for 15 minutes at 121°C using a Systec™ DB23 autoclave or sterilized by filtration using MilliPore 0.22 µm cellulose acetate filters prior to each experiment. Known quantities of previously grown *Synechococcus* sp. were added to the sterile aqueous carbonate solutions of all biotic reactors. Aliquots of 50 mmol/kg aqueous CaCl<sub>2</sub> were then added to all reactors to obtain an overall reactor fluid Ca concentration of 8.5 mmol/kg. Reactors were constantly bubbled with sterile humidified air that was previously passed through sterile MilliPore 0.22 µm cellulose acetate filters, stirred with magnetic stirring bars and kept under continuous 3000 LUX illumination throughout each experiment. Temperature was kept constant at 24°C with

---

<sup>1</sup> Note that the saturation indexes for calcite calculated in this study have substantial uncertainties and are likely overestimated as the thermodynamic properties of the aqueous complexes that may form among Ca<sup>2+</sup>, HCO<sub>3</sub><sup>-</sup> and the various organic and inorganic compounds present in the nutrient medium are not available. As such these potentially forming aqueous complexes are not considered in the chemical speciation calculations performed in this study.

maximum deviations of  $\pm 1^\circ\text{C}$ . Duplicates and abiotic controls were performed at each experimental condition.

The unicellular freshwater cyanobacteria *Synechococcus sp. PCC 7942* used in the experiments were previously cultured under sterile conditions in BG-11 Freshwater Solution Medium. Culturing was performed at room temperature and continuous illumination with a 3000 LUX cool white fluorescence light while bubbling humidified air to achieve constant mixing. Further details about this cyanobacteria are provided by Obst et al. (2009b; 2009a) and Bundeleva et al. (2014a, 2014b). The initial cyanobacterial cultures showed minor heterotrophic cortège (<5 % of the biomass).

### 3.2 Sampling and Analytical methods

The reactors initially contained 900 ml of fluid; fifty ml aliquots of homogenous suspensions were sampled periodically from the reactors in a sterile laminar hood box. The optical density (OD) and pH were measured in these suspension samples, whereas the fluid supernatants were centrifuged for 10 min at 5000 rpm and filtered using a MilliPore 0.45  $\mu\text{m}$  cellulose acetate filter prior to alkalinity, dissolved inorganic carbon (DIC), Ca concentration and  $\delta^{13}\text{C}_{\text{DIC}}$  measurements. Biomass concentration was monitored from the measured suspension sample optical density at the peak absorption of chlorophyll-a (682 nm) after subtracting the contribution of turbidity determined at 750 nm. The Varian Cary50Scan Spectrophotometer used for this analysis allowed simultaneous measurements of these two wavelengths. This approach thereby reduced the contribution of mineral precipitates or cell debris on the OD measurements. Optical density was converted to dry biomass using a linear calibration curve (see Fig A1). The uncertainty of the resulting biomass concentrations was estimated to be  $\pm 10\%$ . The pH was measured using a VWR semi-micro electrode with an uncertainty of  $\pm 0.05$ . Alkalinity was measured following a standard HCl titration procedure

using a Schott TitroLine alpha plus titrator with an uncertainty of  $\pm 2$  %. Dissolved inorganic carbon (DIC) concentrations were measured using a Shimadzu TOC-VCSN carbon Analyzer with an ASI-V sample unit, having a quantification limit of 0.57 ppm and an uncertainty of 3 %. Aqueous calcium concentrations were measured by flame atomic absorption spectroscopy using a Perkin Elmer AAnalysit 400 with an uncertainty of  $\pm 2$  %. Fluids for  $\delta^{13}\text{C}_{\text{DIC}}$  determination were placed into sterile 24 ml amber serum flasks closed with Wheaton Bromobutyl stoppers and aluminum caps to seal them from the atmosphere and stored at 4°C prior to their analyses. Solid samples for carbon isotope analyses were obtained via centrifugation, stored at -80°C and freeze-dried 1-2 weeks after sampling. No  $\text{H}_2\text{O}_2$  treatment of these solids was performed as centrifugation successfully separated mineral precipitates from the biomass due to the higher density of the mineral compared to the organic phase. Sampled solids were characterized by scanning electron microscopy using a Jeol JSM 6360LV and by X-ray diffraction using a G3000 INEL with a  $\text{CuK}\alpha$  source.

The  $\delta^{13}\text{C}$  values of DIC and carbonate minerals were measured at the stable isotope laboratory of the Joanneum Research in Graz, Austria. Details of the analytical procedure can be found in Spötl (2005) and Alemayehu et al. (2011) for the liquids and in Révész and Landwehr (2002), Spötl and Vennemann (2003), Paul and Skrzypek (2007) and Dietzel et al. (2009) for the solids. In brief, the liquid samples were injected into gas tight vials, which were previously flushed with helium gas and preloaded with six droplets of phosphoric acid. For the solids, 200-400  $\mu\text{g}$  of calcite were placed into sealed Exetainer vials, flushed with helium gas to remove residual air and digested in excess pure phosphoric acid for 2 h at 90°C. Acidification converted the total sample inorganic carbonate into gaseous  $\text{CO}_2$ , which was then analyzed using a fully automated peripheral continuous-flow gas preparation Gasbench II device connected to a Finnigan DELTAplus XP mass spectrometer. This acidification approach, first applied by McCrea (1950) and selectively reacts the inorganic carbonate solid limiting the potential

influence of residual organic carbon that might remain on the solids on measured  $\delta^{13}\text{C}_{\text{Calcite}}$  (Oehlerich et al., 2013). The NSB-19 and two in-house lab standards were measured regularly to calibrate the spectrometer. The method of Santrock et al. (1985) was applied for  $^{17}\text{O}$  correction, and the data were processed using the SSH-correction algorithm included in the Thermo Scientific ISODAT 3.0 software package. The analytical reproducibility of  $\delta^{13}\text{C}$  values was  $\pm 0.1 \text{ ‰}$  ( $1\sigma$ ).

The geochemical code PHREEQC (Parkhurst and Appelo, 1999) was used together with its CarbFix database (Voigt et al., 2018) to calculate the chemical speciation and  $\text{CO}_2$  pressure ( $p\text{CO}_2$ ) of the aqueous fluid phase. The standard state adopted in these calculations for solid phases and  $\text{H}_2\text{O}$  is the pure phase, while a hypothetical 1 mol/kg aqueous solution referenced to infinite dilution is chosen for unit activity of aqueous species, both at the temperature and pressure of interest. The Lawrence Livermore National Laboratory aqueous model (Wolery and Daveler, 1992), which uses the extended Debye-Hückel equation (Helgeson, 1969) was used to calculate activity coefficients of aqueous species. Due to i) the low aqueous fluid calcium concentrations compared to the total biomass concentration (up to 1.85  $\text{g}_{(\text{dry})}/\text{kg}$ ), ii) the unknown concentration of metabolic products, and iii) the lack of thermodynamic properties for aqueous complexes that may have formed between the dissolved Ca and these metabolic products, it was not possible to accurately calculate the saturation state of calcite during the experiments. All calculated calcite saturation states are likely overestimates, as they were generated without provision for many of the aqueous complexes that might be present in the reactive aqueous fluids.

## 4. RESULTS

Three distinct experimental series were performed in this study. Each series consisted of one abiotic and two biotic experiments performed over 19 to 35 days. All experiments were initiated with 8.6 mmol/kg Ca present in the reactive aqueous fluid and each biotic experiment was initiated with  $16 \pm 1$  mg/kg of biomass in these fluids. Experimental series SolA was performed in aqueous fluids initially containing 10 mmol/kg  $\text{NaHCO}_3$ , experimental series SolB was performed in aqueous fluids initially containing 50 mmol/kg  $\text{NaHCO}_3$ , and experimental series SolC was performed in aqueous fluids initially containing 25 mmol/kg  $\text{NaHCO}_3$  and 25 mmol/kg  $\text{Na}_2\text{CO}_3$  (see Table 1). The chemical composition of sampled fluids and the carbon isotope composition of dissolved inorganic carbon and calcite in all experiments are listed in Table A1, together with the volume of aqueous fluid and the mass of calcite present in each reactor after each sampling. These results are summarized below.

### *4.1 Chemical evolution of the reactive fluid*

The temporal evolution of biomass, pH, Ca concentrations, and alkalinity are shown in Figs. 2 and 3 for experimental series SolA, SolB, and SolC. Due to its much lower initial alkalinity, SolA exhibited a distinct fluid compositional evolution compared to SolB and SolC.

During the abiotic experiment SolA-1i, aqueous Ca and DIC concentrations decreased due to carbonate precipitation at the onset of the experiment. After 2.8 days of elapsed time these concentrations remained constant at around 5 mmol/kg for aqueous Ca and 3.1 mmol/kg for DIC. From this time, the pH remained constant at  $8.6 \pm 0.1$  after an initial increase from 8.3. During the biotic experiments SolA-2 and SolA-3, the aqueous Ca concentration decreased at the onset of the experiment by the same amount as in the abiotic control, whereas the DIC concentration dropped to near zero. The biomass concentration continually increased during the

experiments from 0.02 to 1.76-1.85 g<sub>(dry)</sub>/kg and the pH in the reactive fluids increased from initially 8.3 to ~10.9 due to the metabolic activity of growing cyanobacteria. This elevated pH resulted in further Ca-carbonate precipitation. From day 4 until day 21, the fluid Ca concentration continuously decreased while DIC remained near zero until the Ca in the fluid phase approached zero. Once the Ca concentrations approached zero, after ~ 20 days of elapsed time, the DIC concentrations increased to final values of 2.8-3.9 mmol/kg.

The temporal evolutions of aqueous Ca and alkalinity concentrations and pH values in experimental series SolB and SolC, as illustrated in Fig. 3 showed distinct chemical evolutions compared to series SolA. These differences are due to their higher initial aqueous carbonate concentrations in these later experimental series, resulting in higher initial calcite saturation states; the initial SI values are provided in Table 1. Consequently, the aqueous Ca concentrations decreased from 8.5 to less than 0.08 mmol/kg during the first hours of all SolB and SolC experiments. The aqueous Ca concentration remained below this value for the remainder of the experiments. These observations indicate that more than 99% of the initial Ca in these reactors precipitated as calcite during the first few hours of the experiments and negligible net calcite dissolution or precipitation occurred after this time. Note, that although little net calcite dissolution or precipitation occurred after the first few hours of these experiment, calcite recrystallisation and/or some dissolution and precipitation resulting in fluid Ca concentration changes of less than 1% of the initial fluid Ca concentrations could have occurred due to the changing concentrations of biomass, alkalinity, and pH

After an initial rapid change from pH 8.6, the pH in the abiotic reactor SolB-1i fluid remained constant at pH 9.6; similarly, after an initial rapid change from pH 10.1, the pH in the abiotic reactor SolC-1i fluid remained constant at 9.8. In the biotic experiment SolB-2, the biomass concentration increased continuously over time from 0.02 to 1.07 g<sub>(dry)</sub>/kg. During experiment SolB-3, the biomass concentration maximized at 0.58 g<sub>(dry)</sub>/kg after 14 days of

elapsed time then decreased to 0.36 g<sub>(dry)</sub>/kg during the last 10 days of experiment. The pH in the biotic SolB experiments (SolB-2 and SolB-3) increased from 8.6 to values as high as 11.9. In the biotic SolC experiments (SolC-2 and SolC-3), the biomass concentration continuously increased from 0.02 to 1.34 g<sub>(dry)</sub>/kg and the pH increased from 10.1 to 10.7-11.1 followed by a decrease in pH to final values of 10.5 and 10.3. Alkalinity during experimental series SolB dropped from an initial value of 51.5 to 33 mmol/kg within the first hour of elapsed time and then increased slightly in the biotic reactors after 8.8 days of elapsed time to 38 and 36 mmol/kg. During experimental series SolC, alkalinity dropped from 71.6 to 57 mmol/kg within the first hour of elapsed time and then began to increase in the biotic reactors after 8.8 days of elapsed time to 68 mmol/kg the end of these experiments. Note that the initial reactive aqueous fluids contained 50 mmol/kg HCO<sub>3</sub><sup>-</sup> (experimental series SolB) and 25 mmol/kg HCO<sub>3</sub><sup>-</sup> + 25 mmol/kg CO<sub>3</sub><sup>2-</sup> (experimental series SolC) and were not in equilibrium with atmospheric CO<sub>2</sub>. Computed pCO<sub>2</sub> values of the initial SolB aqueous fluids ranged from 10<sup>-2.0</sup> to 10<sup>-2.2</sup> atm and were thus significantly higher than atmospheric pCO<sub>2</sub>. As such, immediately after the onset of these experiments, some DIC was lost to the atmosphere through CO<sub>2</sub> outgassing, such that pCO<sub>2</sub> dropped to 10<sup>-3.6</sup> atm during the abiotic experiment SolB-1i. In contrast, the computed fluid phase pCO<sub>2</sub> in the SolC series fluids was initially at 10<sup>-4.3</sup> atm and thus lower than atmospheric pCO<sub>2</sub>. Consequently, some atmospheric CO<sub>2</sub> dissolved into the reactive fluid until atmospheric level of pCO<sub>2</sub> was attained in abiotic experiment SolC-1i (see Fig 4.)

Due to the decrease in aqueous Ca and DIC concentration and the pH evolution over time the calculated SI<sub>calcite</sub> decreased in all experiments. The final calculated saturation index in all experiments ranged from 0.4 to 0.8 suggesting that the fluids were supersaturated throughout the experiments. This result, however, is likely an overestimate due to the likely formation of stable aqueous complexes among aqueous Ca and DIC with the large number of organic and inorganic species present in the reactive fluids. The formation of such aqueous complexes,

which would increase the solubility of calcite, were not taken into account in the saturation index calculations due to the lack of thermodynamic data for these complexes.

#### *4.2 Mineralogy of the precipitated solids*

Calcium carbonate formation was observed in all experiments and evidenced by the decrease in fluid phase Ca and DIC concentrations. All analyzed solids consisted of pure calcite within XRD detection limits (i.e.,  $\pm 1$  wt.% - see Fig A-2). Representative SEM images of the solids after 4.8 days are shown in Fig.5A-D, whereas Fig 5.E-H show solids collected at the end of these experiments. Fig 5A, E and 5C, G show solids collected from abiotic experiments SolB-1i and SolC-1i, respectively. Fig 5B, F and 5D, H show the solids collected from the biotic experiments SolB-3 and SolC-2. The calcite precipitated is hypidiomorphic, with some of the crystals exhibiting rhombohedral shapes. The grain size ranged from 2 to 5  $\mu\text{m}$ . No morphological differences are evident between the solids sampled from abiotic compared to the biotic experiments, nor are there morphological differences in these solids between the early part and the end of the experiments. However, calcite precipitated during experimental series SolB (Fig 5A, B, E, F) are notably smaller ( $\sim 2$   $\mu\text{m}$  diameter) compared to those precipitated during the more initially supersaturated series SolC (Fig 5C, D, G, H), where calcite crystals were on average about 5  $\mu\text{m}$  in diameter.

#### *4.3 Carbon isotope evolution of dissolved inorganic carbon and calcite during experimental series SolA*

As the  $\delta^{13}\text{C}$  values measured in the DIC and calcite during experimental series SolA showed a distinct behavior compared to those in series SolB and SolC, they are described

separately in this section. The temporal evolution of  $\delta^{13}\text{C}_{\text{DIC}}$  and  $\delta^{13}\text{C}_{\text{Calcite}}$  values of SolA-1i, SolA-2 and SolA-3 are shown in Fig 6A and B. The  $\delta^{13}\text{C}_{\text{DIC}}$  values in the abiotic experiment, SolA-1i increased from -6.08 ‰ to -3.66 ‰ during the first 2.8 days of elapsed time. It subsequently remained stable for 20 days then decreased to  $-9.53 \pm 0.45$  ‰ near the end of the experiment. The  $\delta^{13}\text{C}_{\text{Calcite}}$  values during this experiment were constant at  $-3.25 \pm 0.15$  ‰. In contrast, the carbon isotope composition of both the DIC and calcite in the biotic experiments SolA-2 and SolA-3 evolved with time. After an initial increase in  $\delta^{13}\text{C}_{\text{DIC}}$  values of -4.64 ‰ and -6.37 ‰ to +4.25 ‰ and +6.25 ‰, respectively, during the first 4.7 days of these experiments, the  $\delta^{13}\text{C}_{\text{DIC}}$  values became substantially more negative attaining values as low as -24.38 ‰ in SolA-3 after 20.7 days. These negative  $\delta^{13}\text{C}_{\text{DIC}}$  values persisted as long as the DIC concentrations in the fluid remained below 1 mmol/kg. Once calcite precipitation was complete after ~20 days of elapsed time, DIC and  $\delta^{13}\text{C}_{\text{DIC}}$  increased again. In this study, the completion of calcite precipitation is taken to be after at least 99% of the calcium originally present in the reactor had precipitated. Gaps evident in the datasets in Fig. 6A are due to DIC concentrations being too low to measure carbon isotope compositions using our analytical approach. The values of  $\delta^{13}\text{C}_{\text{Calcite}}$  also decreased with time while it precipitated (see Fig 6B). Starting at values of around 0 ‰, the  $\delta^{13}\text{C}_{\text{Calcite}}$  values became progressively more negative reaching values of -6 ‰ at the end of the experiments. It can be seen, however, that  $\delta^{13}\text{C}_{\text{Calcite}}$  values slightly increased during the final days of these biotic experiments.

#### *4.4 Carbon isotope compositions of dissolved inorganic carbon and calcite during experimental series SolB and SolC*

After an initial rapid change, the  $\delta^{13}\text{C}_{\text{DIC}}$  values in the abiotic experiments SolB-1i and SolC-1i remained stable at  $-2.62 \pm 0.18$  ‰ and  $-4.60 \pm 0.36$  ‰, respectively (Fig 7C and 7F). Note

that the carbon isotope ratios of the  $\text{NaHCO}_3$  and  $\text{Na}_2\text{CO}_3$  powders used to produce the aqueous fluids were  $-5.96\text{‰}$  and  $-2.69\text{‰}$ , respectively. The longer-term  $\delta^{13}\text{C}_{\text{DIC}}$  values in SolB-1i were  $\sim 3.3\text{‰}$  higher than that of the bicarbonate used to produce to initial reactive fluids. In contrast, the longer-term  $\delta^{13}\text{C}_{\text{DIC}}$  values of experiment SolC-1i of  $-4.6\text{‰}$  were close to that calculated from a 50/50 mixture of the  $\text{NaHCO}_3$  and  $\text{Na}_2\text{CO}_3$  reagents used to make this fluid.

Similar to the  $\delta^{13}\text{C}_{\text{DIC}}$  values, the calcite precipitated during these abiotic experiments exhibited only small variations in their  $\delta^{13}\text{C}_{\text{Calcite}}$  values after an initial rapid change. In SolB-1i and SolC-1i, the long-term  $\delta^{13}\text{C}_{\text{Calcite}}$  values were  $-4.80\pm 0.20\text{‰}$  and  $-3.15\pm 0.24\text{‰}$ , respectively (Fig 7C and F). Note that the  $\delta^{13}\text{C}_{\text{Calcite}}$  values were higher than the  $\delta^{13}\text{C}_{\text{DIC}}$  value in experiment SolC-1i but lower than the  $\delta^{13}\text{C}_{\text{DIC}}$  value in experiment SolB-1i. This results in  $\Delta^{13}\text{C}_{\text{Calcite-DIC}}$  values of  $-2.15\pm 0.38\text{‰}$  in experiment SolB-1i and  $1.50\pm 0.60\text{‰}$  in experiment SolC-1i.

The isotope composition of dissolved inorganic carbon showed distinctly different trends in the presence or absence of cyanobacteria (see Fig 7). In the biotic experiments SolB-2 and SolB-3, the  $\delta^{13}\text{C}_{\text{DIC}}$  values increased over the first 12 days by more than  $16\text{‰}$  from initial values of  $-7\text{‰}$  to  $+10\text{‰}$  then decreased by  $6\text{--}9\text{‰}$  at the end of the experiment (see Fig 7A). The biotic experiments SolC-2 and SolC-3 showed a similar behavior but the initial  $\delta^{13}\text{C}_{\text{DIC}}$  value increase was delayed by four days and the  $\delta^{13}\text{C}_{\text{DIC}}$  values increased only by around  $10\text{‰}$ , from initial values of  $\sim -5\text{‰}$  to a maximum of  $\sim +6.5\text{‰}$  (Fig 7D). Likewise, the decrease in  $\delta^{13}\text{C}_{\text{DIC}}$  values at the end of the experiments SolC-2 and SolC-3 was less distinct. The observed final  $\delta^{13}\text{C}_{\text{DIC}}$  values were similar in all biotic experiments of the SolB and SolC experimental series at values between  $+3.28\text{‰}$  and  $+3.75\text{‰}$ .

In contrast to the abiotic control experiments, after an initial relatively rapid change during the precipitation of calcite, the  $\delta^{13}\text{C}_{\text{Calcite}}$  values became progressively more positive over time

during the biotic experiments after the calcite precipitation was complete. In SolB-2 and SolB-3, the  $\delta^{13}\text{C}_{\text{Calcite}}$  values increased by 0.5 ‰ to 1.3 ‰ during the last 30 days of the experiment after calcite precipitation was complete (Fig 7B). The increase was less pronounced in SolC-2 and SolC-3, where  $\delta^{13}\text{C}_{\text{Calcite}}$  values increased by 0.7 ‰ and 0.5 ‰ during the last 30 days of the experiment (see Fig 7E). Again, in this study calcite precipitation is considered complete after more than 99% of the calcium initially present in the reactor had precipitated.

## 5. INTERPRETATION

### 5.1 Carbon isotope fractionation during the abiotic experiments

Table A1 provides the measured carbon isotope compositions of all abiotic experiments. The  $\delta^{13}\text{C}_{\text{DIC}}$  values of the abiotic experiments SolA-1i and SolB-1i increase by about 2.7 ‰ and 2.2 ‰ at the beginning of each experiment (see Fig 6A and Fig 7C). These delta values remain close to constant at  $-3.33 \pm 0.93$  ‰ and  $-2.62 \pm 0.18$  ‰, respectively, for at least 18 days following this initial drop. The  $\delta^{13}\text{C}_{\text{DIC}}$  values in these experiments, performed in the absence of cyanobacteria, is initially set by the bicarbonate and carbonate reagents used to produce the initial reactive aqueous fluids and subsequently change due to calcite precipitation and  $\text{CO}_2$  exchange with the atmosphere. Calcite precipitated at the beginning of these experiments due to their supersaturation in the initial reactive fluid. The observed initial increase in the  $\delta^{13}\text{C}_{\text{DIC}}$  values in SolA-1i and SolB-1i is likely dominated by the preferential loss of  $^{12}\text{C}$  during  $\text{CO}_2$  to the atmosphere by degassing. As the  $\text{CO}_2$  in the fluid phase may not have equilibrated with the atmosphere, the consequences of  $\text{CO}_2$  degassing on  $\delta^{13}\text{C}_{\text{DIC}}$  values is modeled by first using mass balance calculations to determine the quantity of  $\text{CO}_2$  degassed. Mass balance calculations, where  $\text{DIC}_{\text{tot}} = \text{DIC}_{\text{initial}} - (\text{DIC}_{\text{lost by degassing}} + \text{DIC}_{\text{precipitated calcite}})$ , indicate that 42% and 30% of the carbon present in the reactors was degassed to the atmosphere during the first

hours of experiments SolA-1i and SolB-1i, respectively. The degassing of these fluids is also consistent with the observed pCO<sub>2</sub> evolution shown in Fig. 4. The effect of degassing on  $\delta^{13}\text{C}_{\text{DIC}}$  values has been calculated using Eqns. (3) and (4) taking account the amount of CO<sub>2</sub> degassed as determined from mass balance calculations. The results of this calculation are provided in Table 2. Since the bulk of degassing occurred rapidly at the beginning of the experiments, the calculated  $10^3 \ln \alpha^{13}\text{C}_{\text{DIC}-\text{CO}_2(\text{g})}$  used for this calculation was that of the initial aqueous fluid. The  $\delta^{13}\text{C}_{\text{DIC}}$  values calculated from the mass balance calculations due to degassing for experiments SolA-1i and SolB-1i are similar to those calculated to be in equilibrium with the atmosphere as well as those measured at steady-state as listed in Table 2.

The calculated  $\Delta^{13}\text{C}_{\text{Calcite}-\text{DIC}}$  values were close to constant from days 5 to 21 at  $+0.06 \pm 1.07$  ‰ in experiment SolA-1i, and close to constant after 5 days at  $-2.07 \pm 0.38$  ‰ in experiment SolB-1i. These values are within the range of previously published calcite – HCO<sub>3</sub><sup>-</sup> equilibrium fractionation factors (e.g., ranging from  $+0.83$  ‰ to  $+1.96$  ‰; Deines et al., 1974; Jimenez-Lopez et al., 2006; Polag et al., 2010; Romanek et al., 1992). Note also that the equilibrium  $\Delta^{13}\text{C}_{\text{Calcite}-\text{DIC}}$  value will likely decrease somewhat as pH increases beyond 9 due to the formation of aqueous carbonate species (e.g., Zhang et al., 1995).

The  $\delta^{13}\text{C}_{\text{DIC}}$  value remained close to constant after 3 days in experiment SolC-1i at  $-4.61 \pm 0.39$  ‰ (see Fig 7C). This is similar to the carbon isotope composition of the Na<sub>2</sub>CO<sub>3</sub>/NaHCO<sub>3</sub> mixture used to prepare the reactive fluid. The calculated  $\Delta^{13}\text{C}_{\text{Calcite}-\text{DIC}}$  over this time in SolC-1i is  $+1.49 \pm 0.60$  ‰ and agrees with previously published calcite – HCO<sub>3</sub><sup>-</sup> equilibrium fractionation factors. The  $\delta^{13}\text{C}_{\text{DIC}}$  value calculated to be in equilibrium with the atmosphere during experiment SolC-1i is listed in Table 2. This value is significantly higher than that measured, suggesting that isotope equilibration between the fluid and the atmosphere was slower than that between the fluid and the precipitating calcite. Note that in contrast to

experiments SolA-1i and SolB1i, negligible carbon loss to the atmosphere was observed from the abiotic reactor SolC-1i according to mass balance calculations.

## *5.2 Carbon isotope fractionation in the presence of cyanobacteria: CO<sub>2</sub> limited calcite precipitation – Experiments SolA-2 and SolA-3*

Mass balance calculations indicate that calcite precipitation during the biotic experiments SolA-2 and SolA-3 is limited by CO<sub>2</sub> dissolution from the atmosphere into the aqueous reactor fluid. The initial 9 mmol/kg DIC present in the reactor was consumed within the first few days of each experiment and the DIC concentrations stayed below 1 mmol/kg in the reactor fluid while calcite continued to precipitate, limited by rate of atmospheric CO<sub>2</sub> input to the aqueous reactor fluid. The DIC concentration again increased only after calcite precipitation was complete (see Fig. 2). The complete precipitation of calcite is indicated by the consumption by precipitation of at least 99% of the initial aqueous calcium present in the reactor. Calcite precipitated at a close to constant rate during its CO<sub>2</sub> limited growth as evidenced by the linear decrease in Ca concentrations over time (see Fig 2C). It is of interest to note that although calcite growth was limited by the low DIC, such was not the case for the biotic activity. In fact, the rate of biomass increase was faster in experiments SolA-2 and SolA-3, compared to experiments SolB-2, SolB-3, SolC-2 and SolC-3 where the DIC was not limited by calcite growth (see Figs. 2 and 3).

The combination of atmospheric CO<sub>2</sub> dissolution, biotic activity, and calcite precipitation resulted in the distinct carbon isotope signatures in the DIC and precipitated calcite as shown in Fig 6A and B. The initial measured  $\delta^{13}\text{C}_{\text{DIC}}$  values of experiments SolA-2 and SolA-3 were similar to that of the Na bicarbonate powder used to make these aqueous solutions. Within the first five days of experiments SolA-2 and SolA-3, these  $\delta^{13}\text{C}_{\text{DIC}}$  values increased

from around -6 ‰ to +6.25 ‰. This increase can be attributed to the preferential uptake of  $^{12}\text{C}$  by photosynthesis producing a fluid enriched in  $^{13}\text{C}$ . This trend stopped when the carbon concentrations of the fluid dropped to near zero. New carbon entering the fluid via  $\text{CO}_2$  dissolution from the atmosphere was rapidly consumed by the precipitating calcite and the measured  $\delta^{13}\text{C}_{\text{DIC}}$  values decreased from -9.4 ‰ to -24.4 ‰ between day 5 and 24. As DIC consumption by the biota would result in more positive  $\delta^{13}\text{C}_{\text{DIC}}$  values, these observations confirm that calcite precipitation is controlled by the kinetics of  $\text{CO}_2$  dissolution into the aqueous fluid phase rather than by the competition for DIC with the biota. Once calcite precipitation stopped, due to the near complete consumption of aqueous calcium, and DIC concentrations increased, the  $\delta^{13}\text{C}_{\text{DIC}}$  values increased to +1.46 ‰ and -3.01 ‰ in SolA-2 and SolA-3, respectively. During the first few days of the experiments, the precipitated calcite had  $\delta^{13}\text{C}_{\text{Calcite}}$  values of around 0 ‰. Subsequently, when calcite precipitation was limited by carbon influx from the atmosphere, the  $\delta^{13}\text{C}_{\text{Calcite}}$  value decreased to less than -6 ‰. This decreasing trend in  $\delta^{13}\text{C}_{\text{Calcite}}$  reflects the corresponding decrease in  $\delta^{13}\text{C}_{\text{DIC}}$  over this time period. Similarly low  $\delta^{13}\text{C}_{\text{Calcite}}$  values were reported in experimental studies in systems where the rapid precipitation of calcite limited by the supply of atmospheric  $\text{CO}_2$  (Clark et al, 1992). Low  $\delta^{13}\text{C}_{\text{Calcite}}$  values are also observed in natural aragonite and calcite travertines (e.g., O'Neil and Barnes, 1971; Clark et al., 1992; Falk et al., 2016). Finally, after the completion of calcite precipitation, an upward temporal trend in  $\delta^{13}\text{C}_{\text{Calcite}}$  values towards calcite-aqueous fluid isotope equilibrium is apparent (see Fig 6B).

### 5.3 Carbon isotope fractionation in the presence of cyanobacteria during experiments SolB-2, SolB-3, SolC-2 and SolC-3

The metabolic activity of the cyanobacteria leads to a distinct variation of the carbon isotopes of dissolved inorganic carbon during experiments SolB-2, SolB-3, SolC-2 and SolC-3. The average doubling time for *Synechococcus* sp. cyanobacteria is 6 to 12 hours (Bernstein et al., 2014). The typical growth curve of this bacteria, however, exhibits a plateau after  $2\pm 1$  week of incubation followed by a decline after 3 weeks of growth (Shirokova et al., 2013, 2015). This growth and decline in biomass is reflected in the  $\delta^{13}\text{C}_{\text{DIC}}$  as a function of time during the experiments (see Fig 7A and D). During photosynthesis, cyanobacteria preferentially consume the light  $^{12}\text{C}$  isotope (e.g., Johnston and Fischer, 2012; O'Leary, 1988) thus significantly increasing  $\delta^{13}\text{C}_{\text{DIC}}$  values over time. This occurred during the first 10-15 days of these biotic experiments, as the  $\delta^{13}\text{C}_{\text{DIC}}$  values increased by 16-17 ‰ in SolB-2 and SolB-3 and by about 12 ‰ in SolC-2 and SolC-3. This strong increase in  $\delta^{13}\text{C}_{\text{DIC}}$  values was followed by a decrease to final values of  $+3.3\pm 0.1$  ‰ in SolB-2 and SolB-3 and  $+3.5\pm 0.3$  ‰ in SolC-2 and SolC-3, respectively.

The close link between photosynthetic activity and the  $\delta^{13}\text{C}_{\text{DIC}}$  values is illustrated in Fig 8A and B. In the abiotic experiments,  $\text{pCO}_2$  was close to equilibrium with respect to the atmosphere and the  $\delta^{13}\text{C}_{\text{DIC}}$  values remained close to constant after an initial change. In the biotic experiments, the production of biomass removed aqueous carbon and increased pH thereby reducing the  $\text{pCO}_2$  in the fluid phase to  $\sim 10^{-8}$  atm. The preferential uptake of  $^{12}\text{C}$  into biomass caused a strong inverse correlation between the  $\delta^{13}\text{C}_{\text{DIC}}$  values and  $\text{pCO}_2$  as shown in Fig 8A. Fig 8B illustrates the correlation between  $\delta^{13}\text{C}_{\text{DIC}}$  values and biomass. With increasing biomass concentration,  $\delta^{13}\text{C}_{\text{DIC}}$  values increased due to photosynthesis until a biomass concentration of about  $0.6 \text{ g}_{(\text{dry})}/\text{kg}$  was reached (arrow 1) and subsequently the  $\delta^{13}\text{C}_{\text{DIC}}$  values decreased due to  $^{12}\text{C}$  input. These observations are in close agreement with those of Mavromatis

et al. (2015), who precipitated hydrous Mg-carbonates in the presence of cyanobacteria in similar experiments and of Pentecost and Spiro (1990), who observed an increase in  $\delta^{13}\text{C}_{\text{DIC}}$  values caused by the photosynthetic activity of a *Rivularia sp.* colony. An increase in  $\delta^{13}\text{C}_{\text{DIC}}$  values during high productivity events can also be observed in natural systems as described by Parker et al. (2010) and Pokrovsky and Shirokova (2013). The decrease in  $\delta^{13}\text{C}_{\text{DIC}}$  values at the end of the experiments (arrow 2 in Fig 8B) might be caused by either 1) cell lysis, death and the subsequent degradation to abiotic carbon species, 2) predominance of respiration over photosynthesis, as common in natural environments (Schulte et al., 2011), 3) the rate of atmospheric  $\text{CO}_2$  influx exceeding photosynthesis or 4) a combination of these processes.

#### 5.4 Carbon isotope fractionation in calcite after its complete precipitation

In all biotic experiments, the  $\delta^{13}\text{C}_{\text{Calcite}}$  values increased after calcite precipitation was complete (see Figs. 6B, 7B and 7E). In the SolA-2 experiments,  $\delta^{13}\text{C}_{\text{Calcite}}$  values increased from -6.39 ‰ to -5.00 ‰ after calcite precipitation was complete during the last 14 days of the experiment. In the SolA-3 experiments,  $\delta^{13}\text{C}_{\text{Calcite}}$  values increased from -5.79 ‰ to -5.56 ‰ over the last 7 days of the experiment. The  $\delta^{13}\text{C}_{\text{Calcite}}$  values measured during the biotic experiments evolved after calcite precipitation was complete from -4.82 ‰ to -4.23 ‰ in SolB-2, from -5.21 ‰ to -3.45 ‰ in SolB-3, from -3.89 ‰ to -2.77 ‰ in SolC-2 and from -3.79 ‰ to -3.03 ‰ in SolC-3. Nevertheless, the calculated  $\Delta^{13}\text{C}_{\text{Calcite-DIC}}$  throughout these biotic experiments remain highly negative due to the large changes in  $\delta^{13}\text{C}_{\text{DIC}}$  values compared to those of  $\delta^{13}\text{C}_{\text{Calcite}}$ , and thus these systems remain strongly out of isotope equilibrium at the end of the experiments. This observation contrasts with those of Mavromatis et al. (2015), who precipitated the hydrous Mg-carbonates dypingite and nesquehonite in similar biotic experiments and observed a co-variance of  $\delta^{13}\text{C}_{\text{DIC}}$  and  $\delta^{13}\text{C}_{\text{Solid}}$  values. The most striking

observation in Mavromatis et al. (2015) is that  $\Delta^{13}\text{C}_{(\text{Hydrous Mg-carbonate})-\text{DIC}}$  remained close to constant and close to isotope equilibrium as the  $\delta^{13}\text{C}_{\text{DIC}}$  values evolved dramatically, even after the precipitation of the hydrous Mg carbonate minerals was complete. This observation requires the continuous equilibration of the carbon isotope composition of these solid and fluid phases. The contrasting behaviors of these hydrous Mg-carbonates compared to that of calcite in the experiments performed in the present study is likely due to the faster mineral fluid reaction rates of these hydrous Mg-carbonates compared to calcite (e.g., Gautier et al., 2014; Harrison et al., 2019; Pokrovsky et al., 2005).

## 6. DISCUSSION

### 6.1 Estimation of carbon isotope exchange rates

It seems likely that the observed enrichment in  $^{13}\text{C}$  in calcite following its precipitation in this study is driven by the large isotope disequilibrium resulting from the preferential uptake of  $^{12}\text{C}$  by cyanobacteria. To a first approximation, the  $\delta^{13}\text{C}_{\text{Calcite}}$  values increase at a constant rate in each experiment following the complete precipitation of calcite in the biotic experiments. Linear regression of these variations are shown in Figs 6B, 7B and 7E; the slopes of these regression lines are provided in Table 3. The  $\delta^{13}\text{C}_{\text{Calcite}}$  values used in these regression calculations are shown in bold italic font in Table A1.

The rate of  $^{13}\text{C}$  transferred to and from the solid can be quantified by taking account of the first derivative of Eqn. (1) with respect to time:

$$\frac{d(^{13/12}\text{C}_{\text{Calcite}})}{dt} = \frac{^{13/12}\text{C}_{V-PDB}}{1000} \cdot \frac{d(\delta^{13}\text{C}_{\text{Calcite}})}{dt}, \quad (6)$$

where  $^{13/12}\text{C}_{V-PDB}$  again refers to the isotope ratio of the *V-PDB* standard;  $^{13/12}\text{C}_{V-PDB} = 0.01118$  (Hayes, 1983),  $^{13/12}\text{C}_{\text{Calcite}}$  designates the indicated atomic C isotope ratio of the

calcite and  $\delta^{13}\text{C}_{\text{Calcite}}$  refers to the measured calcite isotope composition of the calcite in per mil. Because the total mass of  $^{13}\text{C}$  within calcite in the reactor ( $^{13}\text{C}_{\text{Calcite}}$ ) is related to its carbon isotope ratio  $^{13/12}\text{C}_{\text{Calcite}}$ , according to:

$$^{13}\text{C}_{\text{Calcite}} = m_{\text{Calcite}} \cdot \frac{^{13/12}\text{C}_{\text{Calcite}}}{(^{13/12}\text{C}_{\text{Calcite}}+1)}, \quad (7)$$

where  $m_{\text{Calcite}}$  refers to the total mass of calcite in the reactor, it follows that:

$$\frac{d(^{13}\text{C}_{\text{Calcite}})}{dt} = m_{\text{Calcite}} \cdot \frac{^{13/12}\text{C}_{V-PDB}}{1000} \cdot \left( \frac{1}{(^{13/12}\text{C}_{\text{Calcite}}+1)^2} \right) \cdot \frac{d(\delta^{13}\text{C}_{\text{Calcite}})}{dt}. \quad (8)$$

Note that as  $^{13/12}\text{C}_{\text{Calcite}}$  commonly varies by less than  $\pm 5\%$  in natural samples, it can be

assumed to be a constant equal to  $^{13/12}\text{C}_{V-PDB}$  such that  $\left( \frac{1}{(^{13/12}\text{C}_{\text{Calcite}}+1)^2} \right) \approx 0.98$ . Equation

(8) was used together with the average  $^{13/12}\text{C}_{\text{Calcite}}$  values provided in Table 3 and the

$\frac{d(\delta^{13}\text{C}_{\text{Calcite}})}{dt}$  values generated from the linear regressions shown in Figs. 6B, 7B and 7E, to

compute corresponding values of  $\frac{d(^{13}\text{C}_{\text{Calcite}})}{dt}$ . This latter time derivative was normalized to the

total surface area of calcite in the reactors ( $A_{\text{Calcite}}$ ) to obtain the surface area normalized carbon isotope equilibration rate  $r$  according to:

$$r = \frac{d(^{13}\text{C}_{\text{Calcite}})}{dt} \cdot \frac{1}{A_{\text{Calcite}}}. \quad (9)$$

This calculation describes the rate at which the mass of  $^{13}\text{C}$  is transferred into and out of the calcite structure after more than 99% of the total calcium in the reactor has precipitated. Rates generated by this approach have the same dimensions as mineral dissolution and precipitation rates common in the literature,  $\text{mass}/(\text{time} \cdot \text{length}^2)$  (Liu and Dreybrod, 1997; Oelkers et al., 1994). The surface area used to calculate rates in Eqn. (9) was the total geometric surface area approximated assuming that particles are smooth spheres according to:

$$A_{\text{calcite}} = \frac{6 \cdot m_{\text{Calcite}}}{\rho \cdot d}, \quad (10)$$

where  $m_{\text{Calcite}}$  refers to the total mass of calcite present in the reactor,  $\rho$  designates the density of calcite ( $2.715 \times 10^6 \text{ g/m}^3$ ) and  $d$  designates the average grain diameter, estimated from SEM images. Geometric surface areas generated by Eqn (10) differ by less than 4 percent from those calculated assuming the shape of the grains were identical rhombohedrons with the common  $78^\circ$  interface angle. As the calcite grain size is close to constant within the reactor after its precipitation was complete, the mass to surface ratio remains approximately constant. These calculations yield surface area normalized carbon isotope equilibration rates  $r$  ranging from  $1.75 \times 10^{-14}$  to  $1.71 \times 10^{-13} \text{ mol}^{13}\text{C/m}^2/\text{s}$  (see Table 3).

## 6.2 Estimation of the extent of calcite-fluid carbon exchange following the completion of calcite precipitation

An estimate of the fraction of the carbon that was exchanged into and out of the calcite following its precipitation can be made by assuming that 1) the originally precipitated calcite was isotopically homogenous, and 2) a fraction of this calcite was isotopically equilibrated with the fluid after its precipitation. Based on these assumptions, the fraction  $f$  of the carbon in the calcite that was isotopically equilibrated can be calculated from:

$$\delta^{13}\text{C}_{\text{Calcite final}} = f \cdot \delta^{13}\text{C}_{\text{Calcite EQ}} + (1 - f) \cdot \delta^{13}\text{C}_{\text{Calcite i}}, \quad (11)$$

where  $\delta^{13}\text{C}_{\text{Calcite final}}$  designates the measured  $\delta^{13}\text{C}_{\text{Calcite}}$  value at the end of the experiment,  $\delta^{13}\text{C}_{\text{Calcite i}}$  refers to the  $\delta^{13}\text{C}_{\text{Calcite}}$  value immediately after the completion of calcite precipitation and  $\delta^{13}\text{C}_{\text{Calcite EQ}}$  stands for the  $\delta^{13}\text{C}_{\text{Calcite}}$  value in equilibrium with the fluid phase. In this study,  $\delta^{13}\text{C}_{\text{Calcite EQ}}$  values were estimated by adding the equilibrium fractionation factor  $\Delta^{13}\text{C}_{\text{Calcite-HCO}_3^-}$  of 1.96 ‰ (Deines et al., 1974) to the average  $\delta^{13}\text{C}_{\text{DIC}}$

value measured in the reactors after the completion of calcite precipitation. Table 4 shows the results of this calculation for all biotic experiments. These results suggest from 4.0 to 15.2 % of the carbon in the originally precipitated calcite needed to be isotopically equilibrated with the reactive aqueous fluid after calcite had precipitated to match the  $\delta^{13}\text{C}_{\text{Calcite}}$  evolution observed in the experiments. Note that the results of this calculation are rough approximations since  $\delta^{13}\text{C}_{\text{DIC}}$  values constantly evolved during our experiments due to bacterial activity and as the equilibrium fractionation factor will vary somewhat due to the changing pH of the system. Due to uncertainties in equilibrium fractionation factors in part due to the effects of aqueous inorganic carbon speciation, scatter in the data shown in Figs. 6B, 7B and 7E the likely heterogeneities in the originally precipitated calcite, the calculated percentage of re-equilibrated carbon listed in Table 4 likely have uncertainties on the order of  $\pm 50\%$ . Nevertheless the mass of carbon re-equilibrated isotopically exceeds substantially the net mass of carbon dissolved or precipitated during this time in the experiments. Note that the carbon isotope changes considered in the regression calculations were those obtained after more than 99% of the original calcium in the reactor had precipitated. The amount of isotope equilibration reported in Table 4 would require a minimum isotope exchange depth, assuming spherical calcite grains of 2 to 5  $\mu\text{m}$  diameter, of 136 to 801  $\text{\AA}$ .

Insight into the mechanism of post-calcite precipitation carbon exchange can be gained by consideration of the solid-state diffusion rates in calcite. The solid-state diffusion rate of carbon in calcite at 25°C can be calculated using the diffusion coefficient,  $D = 1.6 \times 10^{-32} \text{ m}^2/\text{s}$  (Anderson, 1969). Taking account of this diffusion coefficient, the diffusion length can be estimated using (Bird et al., 1960):

$$x = 2\sqrt{Dt}, \quad (12)$$

where  $x$  designates the characteristic diffusion length as a function of time  $t$  for a diffusion constant  $D$ . This calculation suggests that calcite would retain its carbon isotope signature at

100 Å depth for at least  $5 \times 10^7$  years at 25°C. In contrast, the carbon isotope variations observed in calcite in this study requires substantial isotope exchange at this depth in no more than one month. Due to observations such as this, isotope modification of minerals at ambient temperatures is commonly interpreted to arise from by a grain coarsening or Ostwald ripening mechanism (e.g., Lifshitz and Slyozov 1961). This mechanism thus implies an increase in average crystal size over time as described for example by Kile et al. (2000). Such has not been observed during this study based on SEM investigations of the precipitated calcite at the beginning and the end of the experiment. The changes in grain size, and/or changes in calcite crystallinity may not, however, be observable at the scale of the SEM observations. Another possibility mechanism has been proposed by Putnis (2009) who proposed fluid infiltration of chemical species into the reacting crystals through a porous reaction front generated by interface-coupled dissolution-reprecipitation reactions. The latter is especially pertinent to calcite, given high lability of surface layers of this mineral (Stipp, 1999).

### *6.3 Estimation of carbon isotope equilibration rates in calcite in natural systems*

The results summarized above suggest that carbon isotope re-equilibration between carbonate minerals and its co-existing fluid might occur if a significant isotope disequilibrium exists between these phases. As an illustrative example of the potential implications of the isotope exchange rates generated in this study, the median calcite carbon isotope equilibration rate  $r = 5.29 \times 10^{-14} \text{ mol}^{13}\text{C}/\text{m}^2/\text{s}$  generated above can be used together with Eqns. (8) and (9) to estimate the rates of carbon isotope equilibration in natural systems. For a calcite grain with diameter  $d$ ,  $A_{\text{calcite}}$  can be estimated from Eqn. (10). Multiplying the obtained  $^{13}\text{C}$  equilibration rate by  $A_{\text{Calcite}}$  yields the temporal change in  $^{13}\text{C}$ . This rate can be converted to  $\frac{d(\delta^{13}\text{C}_{\text{Calcite}})}{dt}$  via Eqn. (8) and the time required to change the carbon isotope signature of a

calcite grain by 1‰ can be calculated, provided that it is continuously and substantially out of isotope equilibrium with the fluid phase, for example by a flowing fluid. The results of this calculation as a function of grain diameter from 1 μm to 1 cm are provided in Fig 9. A 1 μm diameter calcite grain in contact with a fluid which is out of isotope equilibrium with this grain is calculated to change its carbon isotope composition by 1 ‰ in 10.8 days whereas it takes about 10<sup>5</sup> days or 296 years to change a calcite grain of 1 cm diameter by 1 ‰. Note that 1) this calculation requires a sufficient large reservoir of DIC, and/or substantial fluid flow to maintain fluid-calcite disequilibria, which may be rare in subsurface systems and 2) the rate of isotope exchange will likely depend on the degree of isotope disequilibrium in the system. Note also, that the rates obtained in this study were normalized to geometric surface area. Total reactive surface area and overall <sup>13</sup>C exchange rates might be notably higher in systems having high surface roughness or nanoporosity (e.g., Mavromatis et al., 2017; Ritter et al., 2017).

The carbon isotope exchange rates generated in this study also suggest that the carbon isotope composition of the fluid phase in carbonate-rich rocks might be strongly affected if it were out of isotope equilibrium with its co-existing solid phases. The carbon isotope evolution of DIC in the presence of calcite depends on the ratio of carbon in the solid to that in the liquid phase. In a system containing solely calcite and an aqueous phase, such as a porous pure limestone, the atomic ratio of carbon in calcite compared to DIC varies as a function of porosity and DIC concentration. Multiplying the average calcite carbon isotope equilibration rate by the surface area of a spherical pore yields the temporal change  $(\frac{d(^{13}C_{calcite})}{dt})$ . Using Eqn. (8), but substituting the total mass of carbon in the pore fluid for  $m_{Calcite}$ , the temporal carbon isotope change  $\frac{d(\text{‰}\delta^{13}C_{DIC})}{dt}$  of the pore fluid can be calculated. Such calculations were used to generate Fig 10A, which shows the calculated time to change the  $\delta^{13}C_{DIC}$  value of a pore fluid by 1 ‰ as a function of the pore diameter assuming that the calcite was continuously and strongly out of isotope equilibrium with the fluid. For this calculation, DIC concentrations of 0.1 mmol/kg,

2 mmol/kg (the concentration of present day seawater) and 5 mmol/kg were considered and the porosity was assumed to be composed of uniform spheres with diameters ranging from 1 to 25 mm. According to these calculations, it would take only 0.8 days to change the  $\delta^{13}\text{C}_{\text{DIC}}$  values by 1 ‰ in a pore fluid having a 2 mmol/kg DIC concentration if the pores had a 1 mm pore diameter and 19.9 days for 25 mm pores.

This result suggests that  $\delta^{13}\text{C}_{\text{DIC}}$  values in limestone could rapidly equilibrate with  $\delta^{13}\text{C}_{\text{Calcite}}$  assuming that  $\delta^{13}\text{C}_{\text{DIC}}$  is not perturbed by other processes such as fluid flow, equilibration with a gas phase or microbial activity/decay. The rapid equilibration of  $\delta^{13}\text{C}_{\text{DIC}}$  values stems from mass balance constraints in these calcite dominated systems; the total carbon in DIC is relatively small compared to the mass of carbon in the calcite in a typical limestone. This is illustrated in Fig. 10B, which shows the atomic ratio of carbon in calcite relative to carbon in the pore fluid having a DIC concentration of 2 mmol/kg. For a hypothetical limestone with 50 % porosity, there is still about  $10^4$  times more C in calcite compared to the pore fluid. Similarly, Han and Plummer (2013) and Han et al. (2014) concluded that the carbon isotope composition of dissolved inorganic carbon in groundwater is ultimately controlled by carbonate minerals due to the considerably larger mass of solid carbonate compared to the mass of DIC. Note, however, our calculations were performed using a representative rate measured in the biotic experiments performed in the present study. The carbon isotopes of the calcite in the present study were as much as 14.3 per mil out of isotope equilibrium with respect to their co-existing fluid phase. It seems likely that the rate of isotope change in calcite will depend on the degree of calcite-aqueous fluid isotope disequilibrium. For example, by analogy with the behavior of mineral dissolution and precipitation rates (Oelkers et al., 1994; Oelkers, 2001), carbon isotope equilibration rates likely decrease as fluid-mineral isotope equilibrium is approached. Some evidence for this is seen in our abiotic experiments. The fluids in our abiotic experiments were closer to isotope equilibrium with their precipitated calcite than our biotic

experiments and the carbon isotope composition of the calcite in these abiotic experiments showed little to no variation after their complete precipitation during the experiments. As such, the results of calculations shown in Fig. 9 and Fig. 10 should be viewed as provisional estimates until a more quantitative description of the rates of isotope variation as a function of isotope disequilibrium become available.

## 7. CONCLUSIONS

The fractionation of carbon isotopes in calcite has been investigated in the presence of actively growing cyanobacteria. The major findings are:

- 1) When calcite precipitation is limited by CO<sub>2</sub> dissolution from the atmosphere into the fluid phase, the fluid and the precipitated solid exhibit highly negative  $\delta^{13}\text{C}$  values despite the presence of cyanobacteria, which would tend to produce a positive DIC and calcite  $\delta^{13}\text{C}$  values due to the preferential uptake of <sup>12</sup>C into biomass. Consequently, the  $\delta^{13}\text{C}$  values of DIC and calcite are significantly more negative than those that might be expected if the system were at equilibrium with the atmosphere. Similar observations were made in systems where rapid carbonate precipitation becomes faster than the dissolution rate of CO<sub>2</sub> gas into the fluid phase such as during the precipitation of dypingite (Wilson et al., 2010) and in natural travertines (Clark et al., 1992; Falk et al., 2016; O'Neil and Barnes, 1971).
- 2) The  $\delta^{13}\text{C}_{\text{Calcite}}$  values were found to evolve towards isotope equilibrium after calcite precipitation was complete at rates ranging from  $1.75 \times 10^{-14}$  to  $1.71 \times 10^{-13}$  mol<sup>13</sup>C/m<sup>2</sup>/s. This carbon isotope exchange rate is much slower than those observed in corresponding experiments of hydrous Mg-carbonates which appear to instantaneously reset their carbon isotope signature (Mavromatis et al., 2015; Harrison et al., 2021).

3) The carbon isotope exchange rates determined in this study are sufficiently fast to significantly modify the carbon isotope signatures of calcite over geologic timespans. Nevertheless, mass balance calculations suggest that in closed systems and in the absence of an internal distinct carbon isotope source (e.g., organic carbon), calcite will preserve its carbon isotope signature by rapidly equilibrating the carbon isotope signature of its co-existing fluid phase. This latter process will, however, tend to rapidly change natural  $\delta^{13}\text{C}_{\text{DIC}}$  values towards isotope equilibrium with their coexisting carbonate minerals if these are out of isotope equilibrium.

### **Acknowledgements**

This research was supported by the Marie Curie EU-FP7 CO2-REACT Research and Training Network. The authors would like to thank Liudmila S. Shirokova, Carole Causserand, Thierry Aigouy and Michel Thibaut for their help with experimental work, wet chemical analyses, SEM- and XRD- measurements, respectively. Anna L. Harrison and Martin Voigt are acknowledged for their helpful ideas and contributions during the edition of this manuscript.

### **References**

- Alemayehu, T., Leis, A., Eisenhauer, A., Dietzel, M., 2011. Multi-proxy approach ( $^2\text{H}/\text{H}$ ,  $^{18}\text{O}/^{16}\text{O}$ ,  $^{13}\text{C}/^{12}\text{C}$  and  $^{87}\text{Sr}/^{86}\text{Sr}$ ) for the evolution of carbonate-rich groundwater in basalt dominated aquifer of Axum area, northern Ethiopia. *Chem. Erde. - Geochem.* 71 (2), 177–187.
- Anderson, T.F., 1969. Self-diffusion of carbon and oxygen in calcite by isotope exchange with carbon dioxide. *J. Geophys. Res.* 74 (15), 3918–3932.
- Andres, M.S., Sumner, D.Y., Reid, R.P., Swart, P.K., 2006. Isotopic fingerprints of microbial respiration in aragonite from Bahamian stromatolites. *Geology* 34 (11), 973–976.
- Archer, D., Maier-Reimer, E., 1994. Effect of deep-sea sedimentary calcite preservation on atmospheric  $\text{CO}_2$  concentration. *Nature* 367, 260–263.

- Assayag, N., Jézéquel, D., Ader, M., Viollier, E., Michard, G., Prévot, F., Agrinier, P., 2008. Hydrological budget, carbon sources and biogeochemical processes in Lac Pavin (France): Constraints from  $\delta^{18}\text{O}$  of water and  $\delta^{13}\text{C}$  of dissolved inorganic carbon. *Appl. Geochem.* 23 (10), 2800–2816.
- Banner, J.L., Hanson, G.N., 1990. Calculation of simultaneous isotopic and trace element variations during water-rock interaction with applications to carbonate diagenesis. *Geochim. Cosmochim. Acta.* 54 (11), 3123–3137.
- Bartley, J.K., Kah, L.C., 2004. Marine carbon reservoir,  $C_{\text{org}}-C_{\text{carb}}$  coupling, and the evolution of the Proterozoic carbon cycle. *Geology* 32 (2), 129–132.
- Beard, B.L., Handler, R.M., Scherer, M.M., Wu, L., Czaja, A.D., Heimann, A., Johnson, C.M., 2010. Iron isotope fractionation between aqueous ferrous iron and goethite. *Earth Planet. Sci. Lett.* 295, 241–250. <https://doi.org/0.1016/j.epsl.2010.04.006>
- Berner, R.A., 1992. Weathering, plants, and the long-term carbon cycle. *Geochim. Cosmochim. Acta.* 56 (8), 3225–3231.
- Berner, R.A., 2004. *The Phanerozoic Carbon Cycle: CO<sub>2</sub> and O<sub>2</sub>*. Oxford University Press.
- Berner, R.A., Lasaga, A.C., Garrels, R.M., 1983. The carbonate-silicate geochemical cycle and its effect on atmospheric carbon dioxide over the past 100 million years. *Am. J. Sci.* 283 (7), 641–683.
- Bernstein, H.C., Konopka, A., Melnicki, M.R., Hill, E.A., Kucek, L.A., Zhang, S., Shen, G., Bryant, D.A., Beliaev, A.S., 2014. Effect of mono- and dichromatic light quality on growth rates and photosynthetic performance of *Synechococcus* sp. PCC 7002. *Front Microbiol.* 5, 488.
- Bird, R.B., Stewart, W.E., Lightfoot, E.N., 1960. *Transport Phenomena*. John Wiley & Sons, New York.
- Botz, R., Pokojski, H.-D., Schmitt, M., Thomm, M., 1996. Carbon isotope fractionation during bacterial methanogenesis by CO<sub>2</sub> reduction. *Org. Geochem.* 25 (3), 255–262.
- Brady, A.L., Druschel, G., Leoni, L., Lim, D.S., Slater, G.F., 2013. Isotopic biosignatures in carbonate-rich, cyanobacteria-dominated microbial mats of the Cariboo Plateau, B.C. *Geobiol.* 11 (5), 437–456.
- Brand, U., Veizer, J., 1980. Chemical diagenesis of a multicomponent carbonate system-1: Trace elements. *J. Sediment. Res.* 50 (4).
- Brand, U., Veizer, J., 1981. Chemical diagenesis of a multicomponent carbonate system-2: Stable isotopes. *J. Sediment. Res.* 51 (3).
- Broecker, W.S., 1970. A boundary condition on the evolution of atmospheric oxygen. *J. Geophys. Res.* 75 (18), 3553–3557.
- Bundeleva, I.A., Ménez, B., Augé, T., Bodéan, F., Recham, N., Guyot, F., 2014a. Effect of cyanobacteria *Synechococcus* PCC 7942 on carbonation kinetics of olivine at 20°C. *Miner. Eng.* 59, 2–11.
- Bundeleva I.A., Shirokova L.S., Pokrovsky O.S., Bénézech P., Menez B., Gerard E., Balor S., 2014b. Experimental modeling of calcium carbonate precipitation by cyanobacterium *Gloeocapsa* sp. *Chem. Geol.* 374–375, 44–60.
- Chanda, P., Gorski, C.A., Oakes, R.L., Fantle, M., 2019. Low temperature stable mineral recrystallization for the fidelity of foraminiferal tests and implications for the fidelity of geochemical proxies. *Earth Planet Sci. Lett.* 506, 428–440.

- Clark, I.D., Fontes, J.-C., Fritz, P., 1992. Stable isotope disequilibria in travertine from high pH waters: Laboratory investigations and field observations from Oman. *Geochim. Cosmochim. Acta.* 56 (5), 2041–2050.
- Deines, P., Langmuir, D., Harmon, R.S., 1974. Stable carbon isotope ratios and the existence of a gas phase in the evolution of carbonate ground waters. *Geochim. Cosmochim. Acta.* 38 (7), 1147–1164.
- Dickson, J.D.A., Coleman, M.L. 1980. Changes in carbon and oxygen isotope composition during limestone diagenesis. *Sedimentology*, 27, 107-118.
- Dietzel, M., Tang, J., Leis, A., Köhler, S.J., 2009. Oxygen isotopic fractionation during inorganic calcite precipitation — Effects of temperature, precipitation rate and pH. *Chem. Geol.* 268 (1), 107–115.
- Eichinger, L., 1983. A Contribution to the Interpretation of  $^{14}\text{C}$  Groundwater Ages Considering the Example of a Partially Confined Sandstone Aquifer. *Radiocarbon* 25 (2), 347–356.
- Epstein, S., Buchsbaum, R., Lowenstam, H.A., Urey, H.C., 1953. Revised Carbonate-Water Isotopic Temperature Scale. *GSA Bulletin* 64 (11), 1315–1326.
- Falk, E.S., Guo, W., Paukert, A.N., Matter, J.M., Mervine, E.M., Kelemen, P.B., 2016. Controls on the stable isotope compositions of travertine from hyperalkaline springs in Oman: Insights from clumped isotope measurements. *Geochim. Cosmochim. Acta.* 192, 1–28.
- Ferris, F.G., Thompson, J.B., Beveridge, T.J., 1997. Modern Freshwater Microbialites from Kelly Lake, British Columbia, Canada. *PALAIOS* 12 (3), 213–219.
- Friedrich, A.J., Beard, B.L., Scherer, M.M., Johnson, C.M., 2014. Determination of the Fe(II)aq–magnetite equilibrium iron isotope fractionation factor using the three-isotope method and a multi-direction approach to equilibrium. *Earth Planet. Sci. Lett.* 391, 77–86. <https://doi.org/10.1016/j.epsl.2014.01.032>
- Gautier, Q., Bénézech, P., Mavromatis, V., Schott, J., 2014. Hydromagnesite solubility product and growth kinetics in aqueous solution from 25 to 75°C. *Geochim. Cosmochim. Acta* 138, 1-20.
- Gonfiantini, R., Zuppi, G.M., 2003. Carbon isotope exchange rate of DIC in karst groundwater. *Chem. Geol.* 197 (1), 319–336.
- Gorski, C.A., Fantle, M.S., 2017. Stable mineral recrystallization in low temperature aqueous systems: A critical review. *Geochim. Cosmochim. Acta.* 198, 439–465.
- Han, L.-F., Plummer, L.N., Aggarwal, P., 2014. The curved  $^{14}\text{C}$  vs.  $\delta^{13}\text{C}$  relationship in dissolved inorganic carbon: A useful tool for groundwater age- and geochemical interpretations. *Chem. Geol.* 387, 111–125.
- Han, L.-F., Plummer, L.N., 2013. Revision of Fontes & Garnier's model for the initial  $^{14}\text{C}$  content of dissolved inorganic carbon used in groundwater dating. *Chem. Geol.* 351, 105–114.
- Harrison A.L., Benezeth P., Schott J., Oelkers E.H., Mavromatis V. 2021. Magnesium and carbon isotope fractionation during hydrated Mg- carbonate mineral phase transformations *Geochim. Cosmochim. Acta* 293, 507-524.
- Harrison, A.L., Mavromatis, V., Oelkers, E.H., Benezeth, P., 2019. Solubility of the hydrated Mg-carbonates nesquehonite and dypingite from 5 to 35 degrees C: Implications for CO<sub>2</sub> storage and the relative stability of Mg-carbonates. *Chem. Geol.* 504, 123-135.

- Hayes, J.M., 1983. Practice and principles of isotopic measurements in organic geochemistry. *Organic geochemistry of contemporaneous and ancient sediments* 5, 1-25.
- Hayes, J.M., Strauss, H., Kaufman, A.J., 1999. The abundance of  $^{13}\text{C}$  in marine organic matter and isotopic fractionation in the global biogeochemical cycle of carbon during the past 800 Ma. *Chem. Geol.* 161 (1), 103–125.
- Helgeson, H.C., 1969. Thermodynamics of hydrothermal systems at elevated temperatures and pressures. *Am. J. Sci.* 267 (7), 729–804.
- Jimenez-Lopez, C., Romanek, C.S., Caballero, E., 2006. Carbon isotope fractionation in synthetic magnesian calcite. *Geochim. Cosmochim. Acta.* 70 (5), 1163–1171.
- Johnston, D.T., Fischer, W.W., 2012. Stable Isotope Geobiology, in: *Fundamentals of Geobiology*. John Wiley & Sons, Ltd, pp. 250–268.
- Kile, D.E., Eberl, D.D., Hoch, A.R., Reddy, M.M., 2000. An assessment of calcite crystal growth mechanisms based on crystal size distributions. *Geochim. Cosmochim. Acta.* 64 (17), 2937–2950.
- Kump, L.R., Arthur, M.A., 1999. Interpreting carbon-isotope excursions: Carbonates and organic matter. *Chem. Geol.* 161 (1), 181–198.
- Lifshitz, I.M., Slyozov, V.V., 1961. The kinetics of precipitation from supersaturated solid solutions. *J. Phys. Chem. Solids* 19 (1), 35–50.
- Li, W., Beard, B.L., Johnson, C.M., 2011. Exchange and fractionation of Mg isotopes between epsomite and saturated  $\text{MgSO}_4$  solution. *Geochim. Cosmochim. Acta* 75, 1814–1828. <https://doi.org/10.1016/j.gca.2011.01.023>
- Liu, Z., Dreybrod, W., 1997. Dissolution kinetics of calcium carbonate minerals in  $\text{H}_2\text{O}-\text{CO}_2$  solutions in turbulent flow: The role of the diffusion boundary layer and the slow reaction  $\text{H}_2\text{O} + \text{CO}_2 \rightarrow \text{H}^+ + \text{HCO}_3^-$ . *Geochim. Cosmochim. Acta.* 61 (14), 2879–2889.
- Mavromatis, V., Bundeleva, I.A., Shirokova, L.S., Millo, C., Pokrovsky, O.S., Bénézech, P., Ader, M., Oelkers, E.H., 2015. The continuous re-equilibration of carbon isotope compositions of hydrous Mg carbonates in the presence of cyanobacteria. *Chem. Geol.* 404, 41–51.
- Mavromatis, V., Pearce, C.R., Shirokova, L.S., Bundeleva, I.A., Pokrovsky, O.S., Benezeth, P., Oelkers, E.H., 2012. Magnesium isotope fractionation during hydrous magnesium carbonate precipitation with and without cyanobacteria. *Geochim. Cosmochim. Acta.* 76, 161–174.
- Mavromatis, V., Harrison, A.L., Eisenhauer, A., Dietzel, M., 2017. Strontium isotope fractionation during strontianite ( $\text{SrCO}_3$ ) dissolution, precipitation and at equilibrium. *Geochim. Cosmochim. Acta* 218, 201-214.
- Mavromatis, V., van Zuilen, K., Purgstaller, B., Baldermann, A., Nägler, T.F., Dietzel, M., 2016. Barium isotope fractionation during witherite ( $\text{BaCO}_3$ ) dissolution, precipitation and at equilibrium. *Geochim. Cosmochim. Acta.* 190, 72–84.
- McCrea, J.M., 1950. On the Isotopic Chemistry of Carbonates and a Paleotemperature Scale. *J. Chem. Phys.* 18 (6), 849–857.
- McDermott, F., 2004. Palaeo-climate reconstruction from stable isotope variations in speleothems: A review. *Quat. Sci. Rev.* 23 (7), 901–918.
- Merz, M.U.E., 1992. The biology of carbonate precipitation by cyanobacteria. *Facies* 26, 81-102.

- Mozeto, A.A., Fritz, P., Reardon, E.J., 1984. Experimental observations on carbon isotope exchange in carbonate-water systems. *Geochim. Cosmochim. Acta.* 48 (3), 495–504.
- Myrntinen, A., Becker, V., Barth, J.A.C., 2012. A review of methods used for equilibrium isotope fractionation investigations between dissolved inorganic carbon and CO<sub>2</sub>. *Earth-Sci. Rev.* 115 (3), 192–199.
- Obst, M., Dynes, J.J., Lawrence, J.R., Swerhone, G.D.W., Benzerara, K., Karunakaran, C., Kaznatcheev, K., Tyliszczak, T., Hitchcock, A.P., 2009a. Precipitation of amorphous CaCO<sub>3</sub> (aragonite-like) by cyanobacteria: A STXM study of the influence of EPS on the nucleation process. *Geochim. Cosmochim. Acta.* 73 (14), 4180–4198.
- Obst, M., Wehrli, B., Dittrich, M., 2009b. CaCO<sub>3</sub> nucleation by cyanobacteria: Laboratory evidence for a passive, surface-induced mechanism. *Geobiol.* 7 (3), 324–347.
- Oehlerich, M., Baumer, M., Lucke, A., Mayr, C., 2013. Effect of organic matter of carbonate stable isotope ratios ( $\delta^{13}\text{C}$ ,  $\delta^{18}\text{O}$  values) - Implications for analyses of bulk sediments. *Rapid Comm. Mass Spectro.*, 27, 707-712.
- Oelkers, E.H., 2001. General kinetic description of multioxide silicate mineral and glass dissolution. *Geochim. Cosmochim. Acta.* 65 (21), 3703–3719.
- Oelkers, E.H. Pogge von Strandmann, P.A.E., Mavromatis, V. 2019. The rapid resetting of the Ca isotope signatures of calcite at ambient temperatures during its congruent dissolution, precipitation, and at equilibrium. *Chem. Geol.*, 512, 1-10.
- Oelkers, E.H., Schott, J., Devidal, J.-L., 1994. The effect of aluminum, pH, and chemical affinity on the rates of aluminosilicate dissolution reactions. *Geochim. Cosmochim. Acta.* 58 (9), 2011–2024.
- O'Leary, M.H., 1988. Carbon Isotopes in Photosynthesis. *BioScience* 38 (5), 328–336.
- O'Neil, J.R., Barnes, I., 1971. C<sup>13</sup> and O<sup>18</sup> compositions in some freshwater carbonates associated with ultramafic rocks and serpentinites: Western United States. *Geochim. Cosmochim. Acta.* 35 (7), 687–697.
- Parker, S.R., Gammons, C.H., Poulson, S.R., DeGrandpre, M.D., Weyer, C.L., Smith, M.G., Babcock, J.N., Oba, Y., 2010. Diel behavior of stable isotopes of dissolved oxygen and dissolved inorganic carbon in rivers over a range of trophic conditions, and in a mesocosm experiment. *Chem. Geol.* 269 (1), 22–32.
- Parkhurst, D.L., Appelo, C.A.J., 1999. User's guide to PHREEQC (Version 2): A computer program for speciation, batch-reaction, one-dimensional transport, and inverse geochemical calculations. *Water-Resources Investigations Report* 99-4259.
- Paul, D., Skrzypek, G., 2007. Assessment of carbonate-phosphoric acid analytical technique performed using GasBench II in continuous flow isotope ratio mass spectrometry. *Int. J. Mass Spectrom.* 262 (3), 180–186.
- Pederson, C., Mavromatis, V., Dietzel, M., Rollion-Bard, C., Nehrke, G., Jons, N., Jochum, K.P., Immenhauser, A., 2019. Diagenesis of mollusc aragonite and the role of fluid reservoirs. *Earth Planet. Sci. Lett.* 514, 130-142.
- Pentecost, A., Spiro, B., 1990. Stable carbon and oxygen isotope composition of calcites associated with modern freshwater cyanobacteria and algae. *Geomicrobil. J.* 8 (1), 17–26.
- Pokrovsky, O.S., Golubev, S.V., Schott, J., 2005. Dissolution kinetics of calcite, dolomite and magnesite at 25 °C and 0 to 50 atm pCO<sub>2</sub>. *Chem. Geol.*, 217, 239-255.

- Pokrovsky, O.S., Shirokova, L.S., 2013. Diurnal variations of dissolved and colloidal organic carbon and trace metals in a boreal lake during summer bloom. *Water. Res.* 47 (2), 922–932.
- Polag, D., Scholz, D., Mühlinghaus, C., Spötl, C., Schröder-Ritzrau, A., Segl, M., Mangini, A., 2010. Stable isotope fractionation in speleothems: Laboratory experiments. *Chem. Geol.* 279 (1), 31–39.
- Power, I.M., Wilson, S.A., Dipple, G.M., Southam, G., 2011. Modern carbonate microbialites from an asbestos open pit pond, Yukon, Canada. *Geobiol.* 9 (2), 180–195.
- Putnis, A., 2009. Mineral Replacement Reactions. *Rev. Mineral. Geochem.* 70 (1), 87–124.
- Révész, K.M., Landwehr, J.M., 2002.  $\delta^{13}\text{C}$  and  $\delta^{18}\text{O}$  isotopic composition of  $\text{CaCO}_3$  measured by continuous flow isotope ratio mass spectrometry: Statistical evaluation and verification by application to Devils Hole core DH-11 calcite. *Rapid Commun. Mass Spectrom.* 16 (22), 2102–2114.
- Riding, R., 2006. Cyanobacterial calcification, carbon dioxide concentrating mechanisms, and Proterozoic-Cambrian changes in atmospheric composition. *Geobiology*, 4, 29-316.
- Ritter, A.-C., Mavromatis, V., Dietzel, M., Kwiecien, O., Wiethoff, F., Griesshaber, E., Casella, L.A., Schmahl, W.W., Koelen, J., Neuser, R.D., Leis, A., Buhl, D., Niedermayr, A., Breitenbach, S.F., Bernasconi, S.M., Immenhauser, A., 2017. Exploring the impact of diagenesis on (isotope) geochemical and microstructural alteration features in biogenic aragonite. *Sedimentology* 64 (5), 1354–1380.
- Romanek, C.S., Grossman, E.L., Morse, J.W., 1992. Carbon isotopic fractionation in synthetic aragonite and calcite: Effects of temperature and precipitation rate. *Geochim. Cosmochim. Acta.* 56 (1), 419–430.
- Santrock, J., Studley, S.A., Hayes, J.M., 1985. Isotopic analyses based on the mass spectra of carbon dioxide. *Analytical Chemistry* 57 (7), 1444–1448.
- Schidlowski, M., Junge, C.E., 1981. Coupling among the terrestrial sulfur, carbon and oxygen cycles: Numerical modeling based on revised Phanerozoic carbon isotope record. *Geochim. Cosmochim. Acta.* 45 (4), 589–594.
- Schrag, D.P., Higgins, J.A., Macdonald, F.A., Johnston, D.T., 2013. Authigenic Carbonate and the History of the Global Carbon Cycle. *Science* 339 (6119), 540–543.
- Schulte, P., van Geldern, R., Freitag, H., Karim, A., Négrel, P., Petelet-Giraud, E., Probst, A., Probst, J.-L., Telmer, K., Veizer, J., Barth, J.A.C., 2011. Applications of stable water and carbon isotopes in watershed research: Weathering, carbon cycling, and water balances. *Earth-Sci. Rev.* 109 (1), 20–31.
- Shirokova, L.S., Kunhel L., Rols J.-L., Pokrovsky, O.S., 2015. Experimental modeling of cyanobacterial bloom in a thermokarst lake. *Aquatic Geochemistry*, 21(6), 487-511.
- Shirokova, L.S., Mavromatis, V., Bundeleva, I., Pokrovsky, O.S., Benezeth, P., Pearce, C., Oelkers, E.H., 2013. Using Mg isotopes to trace cyanobacterially mediated magnesium carbonate precipitation in alkaline lakes. *Aquatic Geochemistry*, 19, 1-24.
- Spötl, C., 2005. A robust and fast method of sampling and analysis of  $\delta^{13}\text{C}$  of dissolved inorganic carbon in ground waters. *Isot. Environ. Health Stud.* 41 (3), 217–221.
- Spötl, C., Vennemann, T.W., 2003. Continuous-flow isotope ratio mass spectrometric analysis of carbonate minerals. *Rapid Commun. Mass Spectrom.* 17 (9), 1004–1006.

- Stamm, F.M., Zambardi, T., Chmeleff, J., Schott, J., von Blanckenburg, F., Oelkers, E.H., 2019. The experimental determination of equilibrium Si isotope fractionation factors among  $\text{H}_4\text{SiO}_4^0$ ,  $\text{H}_3\text{SiO}_4^-$  and amorphous silica ( $\text{SiO}_2 \cdot 0.32 \text{H}_2\text{O}$ ) at 25 and 75 °C using the three-isotope method. *Geochim. Cosmochim. Acta* 255, 49–68.
- Stamm, F.M., Meheut, M., Zambardi, T., Chmeleff, J., Schott, J., Oelkers, E.H., 2020. Extreme silicon isotope fractionation due to Si organic complexation: Implications for silica biomineralization. *Earth Planet. Sci. Lett.* 542, 116287. 255, 49–68.
- Stipp, S.L.S., 1999. Toward a conceptual model of the calcite surface: Hydration, hydrolysis, and surface potential. *Geochim. Cosmochim. Acta* 63(19-20), 3121-3131.
- Swart, P.K., 2015. The geochemistry of carbonate diagenesis: The past, present and future. *Sedimentology* 62 (5), 1233–1304.
- Urey, H.C., Lowenstam, H.A., Epstein, S., McKinney, C.R., 1951. Measurement of paleotemperatures and temperatures of the Upper Cretaceous of England, Denmark, and the southeastern United States. *Bull. Geol. Soc. Am.* 62 (4), 399–416.
- Voigt, M., Marieni, C., Clark, D.E., Gíslason, S.R., Oelkers, E.H. 2018. Evaluation and refinement of thermodynamic databases for mineral carbonation. *Energy Procedia* 146, 81-91
- Wendt, I., 1971. Carbon and oxygen isotope exchange between  $\text{HCO}_3^-$  in saline solution and solid  $\text{CaCO}_3$ . *Earth Planet. Sci. Lett.* 12 (4), 439–442.
- Whiticar, M.J., 1999. Carbon and hydrogen isotope systematics of bacterial formation and oxidation of methane. *Chem. Geol.* 161 (1), 291–314.
- Wilson, S.A., Barker, S.L., Dipple, G.M., Atudorei, V., 2010. Isotopic disequilibrium during uptake of atmospheric  $\text{CO}_2$  into mine process waters: Implications for  $\text{CO}_2$  sequestration. *Environ. Sci. Technol.* 44 (24), 9522–9529.
- Wolery, T.J., Daveler, S.A., 1992. EQ6, a computer program for reaction path modeling of aqueous geochemical systems: Theoretical manual, user's guide and related documentation (Version 7.0). Lawrence Livermore Laboratory, University of California Livermore, CA.
- Wynn, J.G., Bird, M.I., Wong, V.N.L., 2005. Rayleigh distillation and the depth profile of  $^{13}\text{C}/^{12}\text{C}$  ratios of soil organic carbon from soils of disparate texture in Iron Range National Park, Far North Queensland, Australia. *Geochim. Cosmochim. Acta.* 69 (8), 1961–1973.
- Zhang, J., Quay, P.D., Wilbur, D.O., 1995. Carbon isotope fractionation during gas-water exchange and dissolution of  $\text{CO}_2$ . *Geochim. Cosmochim. Acta.* 59 (1), 107–114.

**Table 1.** Summary of experimental conditions of all experiments performed in this study.

Initial Conditions:

Experiment ID	Experiment Duration (days)	NaHCO <sub>3</sub> (mmol/kg)	Na <sub>2</sub> CO <sub>3</sub> (mmol/kg)	CaCl <sub>2</sub> (mmol/kg)	SI calcite	BG-11 (g/kg)	biomass (g <sub>(dry)</sub> /kg)
SolA-1i	35	10		8.6	1.8	20	
SolA-2	35	10		8.6	1.8	20	0.016
SolA-3	35	10		8.6	1.8	20	0.015
SolB-1i	19	50		8.5	2.6	20	
SolB-2	33	50		8.5	2.6	20	0.017
SolB-3	33	50		8.5	2.6	20	0.017
SolC-1i	26	25	25	8.5	3.0	20	
SolC-2	33	25	25	8.5	3.0	20	0.017
SolC-3	33	25	25	8.5	3.0	20	0.017

Conditions during experiment:

Experiment ID	Biomass range (g <sub>(dry)</sub> /kg)	pH range	Ca conc. range (mmol/kg)	DIC range (mmol/kg)	Alkalinity range (mmol/kg)
SolA-1i	abiotic	8.31 - 8.68	8.63 - 4.89	9.05 - 3.11	
SolA-2	0.016 - 1.852	8.32 - 10.76	8.60 - 0.10	9.10 - 0.28	
SolA-3	0.015 - 1.755	8.26 - 10.94	8.53 - 0.05	9.05 - 0.23	
SolB-1i	abiotic	8.31 - 9.60	8.50 - 0.02	46.9 - 27.4	51.5 - 32.1
SolB-2	0.017 - 1.070	8.20 - 11.65	8.50 - 0.02	46.9 - 20.2	51.5 - 32.4
SolB-3	0.017 - 0.357	8.25 - 11.85	8.50 - 0.02	46.9 - 19.5	51.5 - 33.3
SolC-1i	abiotic	9.76 - 10.14	8.50 - 0.01	48.8 - 44.3	71.6 - 56.1
SolC-2	0.017 - 1.339	9.92 - 11.12	8.50 - 0.02	47.7 - 28.9	71.6 - 57.1
SolC-3	0.017 - 1.342	9.89 - 10.73	8.50 - 0.03	47.7 - 39.7	71.6 - 56.7

**Table 2.** Measured and calculated carbon isotope fractionation in the abiotic experiments. The calculated initial values are determined from the isotope composition of the reagents used to produce the initial reactive fluids together with mass balance constraints. The calculated compositions in equilibrium with atmospheric CO<sub>2</sub> and after CO<sub>2</sub> degassing were determined according to Eqns. (2) and (3). The carbon isotope composition of the atmosphere was taken to be  $\delta^{13}\text{C}_{\text{CO}_2} = -8.5 \pm 1\text{‰}$  (Mavromatis et al., 2015).

ID	$\delta^{13}\text{C}_{\text{DIC}}$ (‰)					$\delta^{13}\text{C}_{\text{Calcite}}$ (‰)	$\Delta^{13}\text{C}_{\text{Calcite-DIC}}$ <sup>1</sup>
	Measured initial	Calculated from the initial powder	Measured average steady-state	Calculated in equilibrium with CO <sub>2(atm)</sub>	Calculated from mass balance after initial C loss	Measured average steady-state <sup>a</sup>	
SolA-1i	-6.08 ± 0.1	-5.96 ± 0.1 <sup>2</sup>	-3.33 ± 0.93 <sup>3</sup>	-0.72 ± 1	-1.88	-3.27 ± 0.15	+0.06 ± 1.07
SolB-1i	-4.74 ± 0.1	-5.96 ± 0.1	-2.66 ± 0.18	-1.85 ± 1	-2.27	-4.73 ± 0.20	-2.07 ± 0.38
SolC-1i	-4.31 ± 0.1	-4.33 ± 0.1	-4.53 ± 0.36	-2.47 ± 1	no C loss	-3.03 ± 0.24	+1.50 ± 0.60

1) Difference of averaged steady state values

2) Determined from the mass weighted sum of the  $\delta^{13}\text{C}$  values of the NaHCO<sub>3</sub> and Na<sub>2</sub>CO<sub>3</sub> powders used to make the initial solution; the  $\delta^{13}\text{C}$  values of these NaHCO<sub>3</sub> and Na<sub>2</sub>CO<sub>3</sub> powders were -5.96 ‰ and -2.69 ‰, respectively.

3) Average value from day 5 to day 21

**Table 3.** Estimated carbon isotope equilibration rates normalized to geometric surface area ( $r$ ). The  $\frac{d(\delta^{13}\text{C}_{\text{Calcite}})}{dt}$  values in ‰/s were obtained by linear regression of the  $\delta^{13}\text{C}_{\text{Calcite}}$  measurements as shown in Figs. 6 and 7. Calcite crystal diameters  $d$  were estimated from SEM images to estimate geometric surface area  $A_{\text{calcite}}$ .  $^{13/12}\text{C}_{\text{Calcite}}(t_i)$  and  $^{13/12}\text{C}_{\text{Calcite}}(t_e)$  designate the calculated  $^{13/12}\text{C}$  at the beginning ( $t_i$ ) of the carbon isotope re-equilibration and the end ( $t_e$ ) of the experiment.

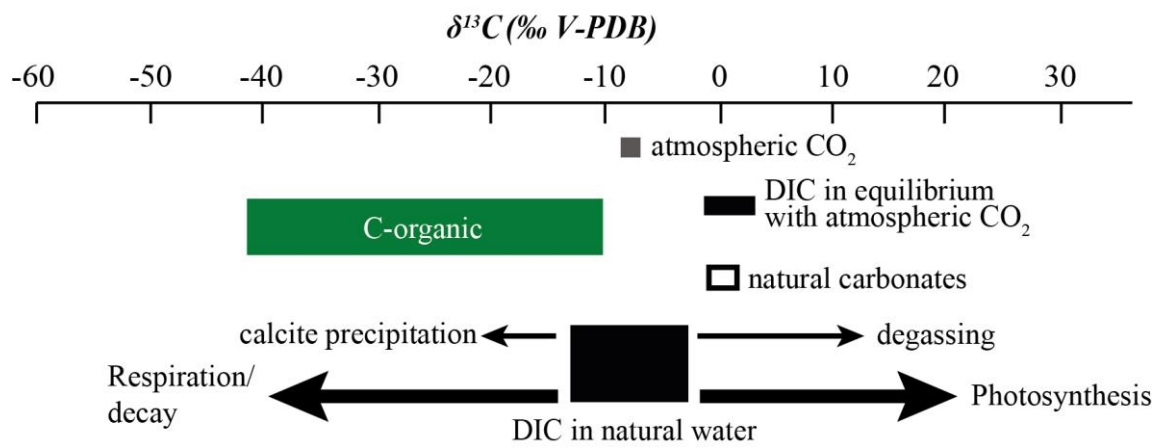
ID	$\frac{d(\delta^{13}\text{C}_{\text{Calcite}})}{dt}$ (‰/s) x $10^{-7}$	$^{13/12}\text{C}_{\text{Calcite}}(t_i)$	$^{13/12}\text{C}_{\text{Calcite}}(t_e)$	$r$ (mol $^{13}\text{C}/\text{m}^2/\text{s}$ ) x $10^{-14}$
SolA-2	11.6 ± 0.72	0.011109	0.011125	17.1 ± 4.26
SolA-3	3.68 ± 1.34	0.011116	0.011118	5.45 ± 17.8
SolB-2	1.77 ± 1.00	0.011128	0.011134	1.75 ± 1.31
SolB-3	5.19 ± 0.95	0.011124	0.011139	5.13 ± 1.31
SolC-2	2.87 ± 0.66	0.011142	0.011151	7.09 ± 2.07
SolC-3	1.88 ± 0.71	0.011142	0.011148	4.64 ± 2.23

ID	Time elapsed ( $t_i$ - $t_e$ ) (days)	Calcite diameter $d$ ( $\mu\text{m}$ )	$m_{\text{Calcite}}$ in reactor (mmol)	$A_{\text{tot}}$ in reactor ( $\text{m}^2$ )
SolA-2	14	3	4.78 - 3.02	0.22 - 0.35
SolA-3	7	3	3.98 - 3.04	0.22 - 0.29
SolB-2	32	2	7.01 - 2.76	0.31 - 0.78
SolB-3	31	2	6.93 - 2.75	0.30 - 0.77
SolC-2	33	5	7.13 - 2.75	0.12 - 0.32
SolC-3	33	5	7.07 - 2.75	0.12 - 0.31

**Table 4.** Parameters used and results for the calculations of percentage calcite exchanged and the corresponding carbon exchange depth from the calcite-fluid interface expressed as distance in Å. The percent calcite exchanged corresponds to the fraction  $f$  calculated using Eqn. (11).

ID	Calcite diameter $d$ ( $\mu\text{m}$ )	$\delta^{13}\text{C}_{\text{Calcite i}}$ (‰ V-PDB)	$\delta^{13}\text{C}_{\text{Calcite end}}$ (‰ V-PDB)	$\delta^{13}\text{C}_{\text{Calcite EQ}}$ (‰ V-PDB)	Average	Calcite exchanged $f$ (%)	Depth of C exchange (Å)
					$\delta^{13}\text{C}_{\text{DIC}}$ (‰ V-PDB)		
SolA-2	3	-6.39	-5.00	2.76	0.80	15.2	801
SolA-3	3	-5.79	-5.56	-0.78	-2.74	4.6	233
SolB-2	2	-4.66	-4.19	6.98	5.02	4.0	136
SolB-3	2	-5.05	-3.66	5.89	3.93	12.7	443
SolC-2	5	-3.46	-2.65	5.29	3.33	9.3	797
SolC-3	5	-3.38	-2.86	6.15	4.19	5.5	463



**Fig. 1.** Carbon isotope signatures of various components of the carbon cycle. The grey symbol indicates gaseous carbon, the green box corresponds to organic carbon, the filled black symbols represent carbon in DIC and the black open symbols indicate carbon in carbonate minerals. Arrows indicate processes effecting  $\delta^{13}\text{C}$  (modified from Schulte et al., 2011).

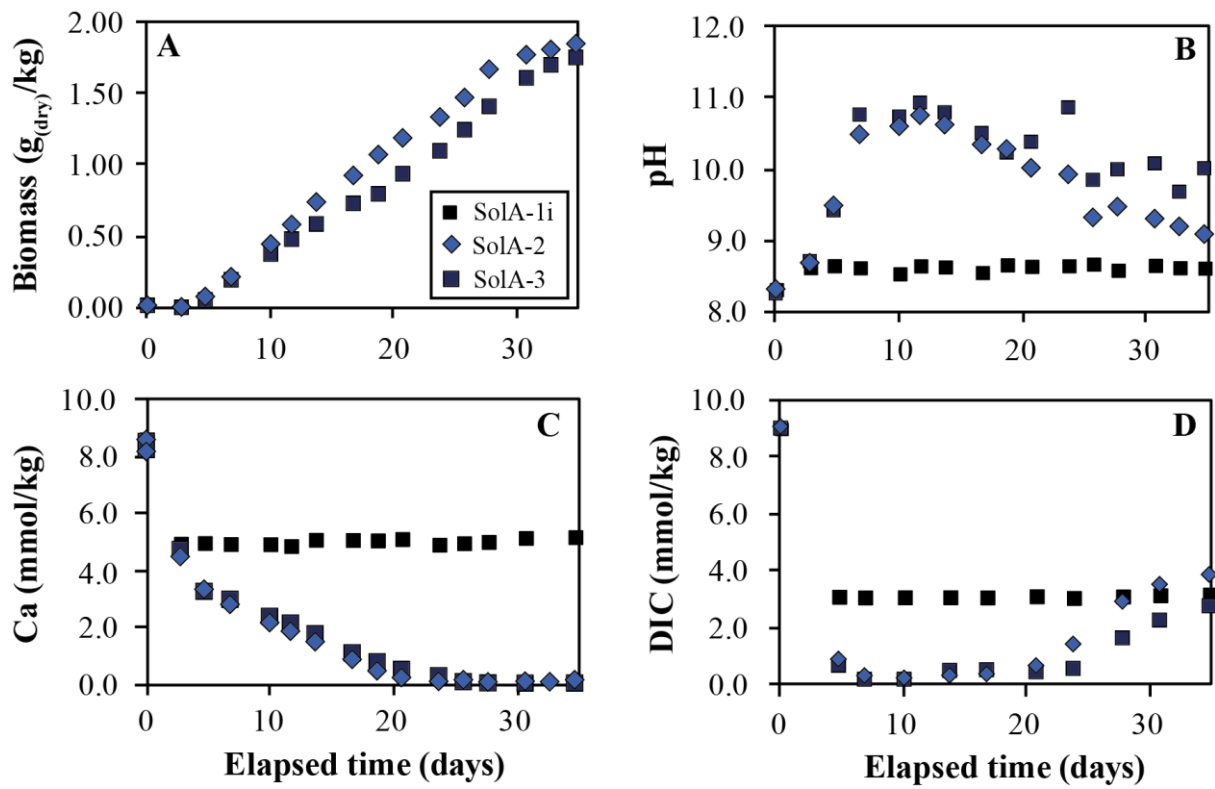


**Fig. 2.** The temporal evolution of biomass concentration (A), pH (B), Ca concentration (C) and DIC (D) during experimental series SolA. The uncertainty of biomass concentration is  $\pm 10\%$  whereas the analytical uncertainties of pH, Ca concentration and DIC are smaller than the symbol sizes. The symbols are identified in Fig. 2A.

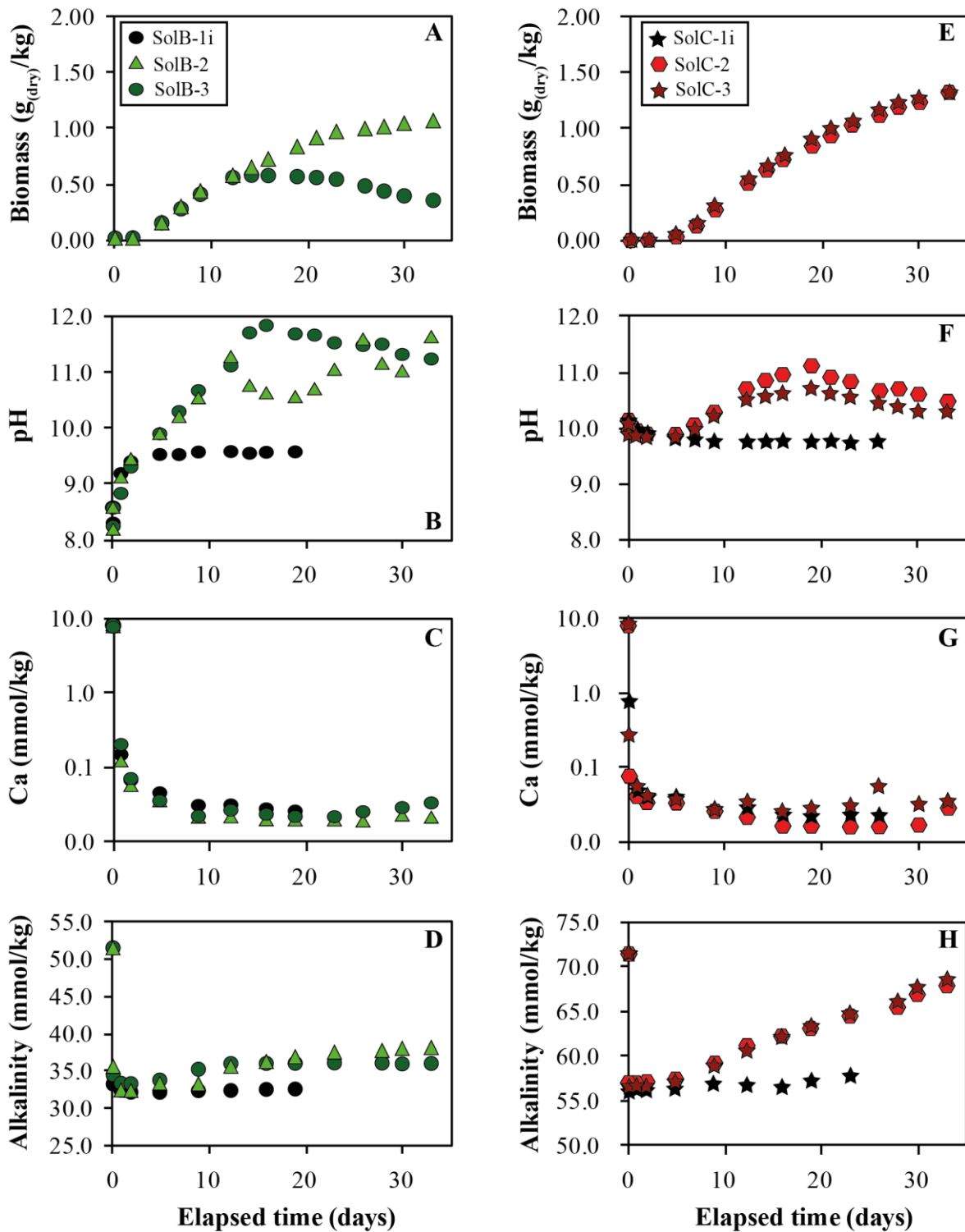


**Fig. 3.** The temporal evolution of biomass concentration (A, E), pH (B, F), Ca concentration (C, G) and alkalinity (D, H) during experimental series SolB and SolC. Note that Ca concentrations are shown on logarithmic scale. The uncertainty of biomass concentration is  $\pm 10\%$  whereas analytical uncertainties on pH, Ca concentrations and alkalinities are smaller than the symbol sizes. The symbols are identified in Figs. 3A and E.

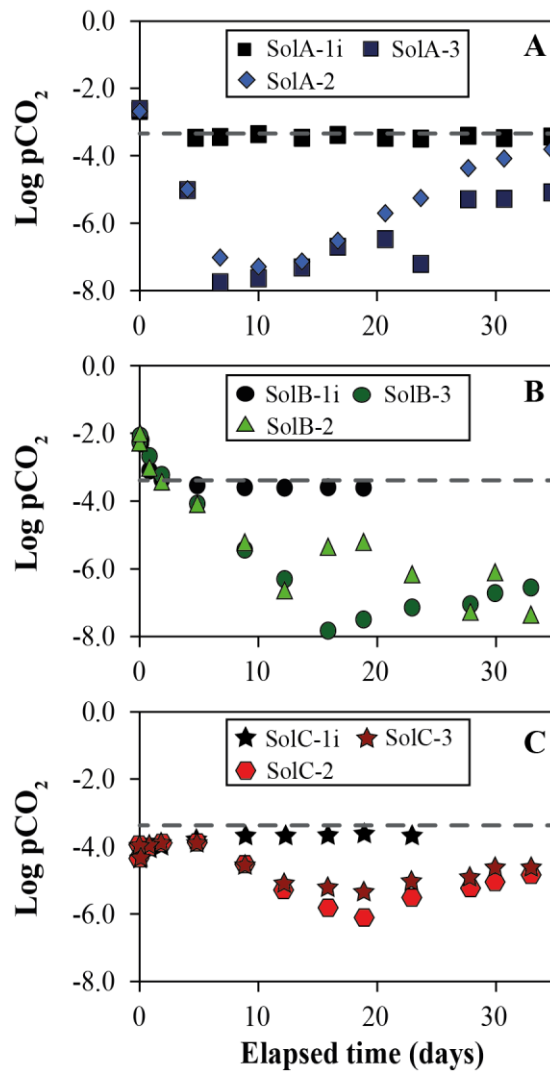


**Fig. 4.** The temporal evolution of  $\text{pCO}_2$  during experimental series SolA (A), SolB (B) and SolC (C).  $\text{pCO}_2$  was calculated from measured aqueous fluid composition using PHREEQC. The symbols are identified in the figures. Dashed lines indicated atmospheric saturation.

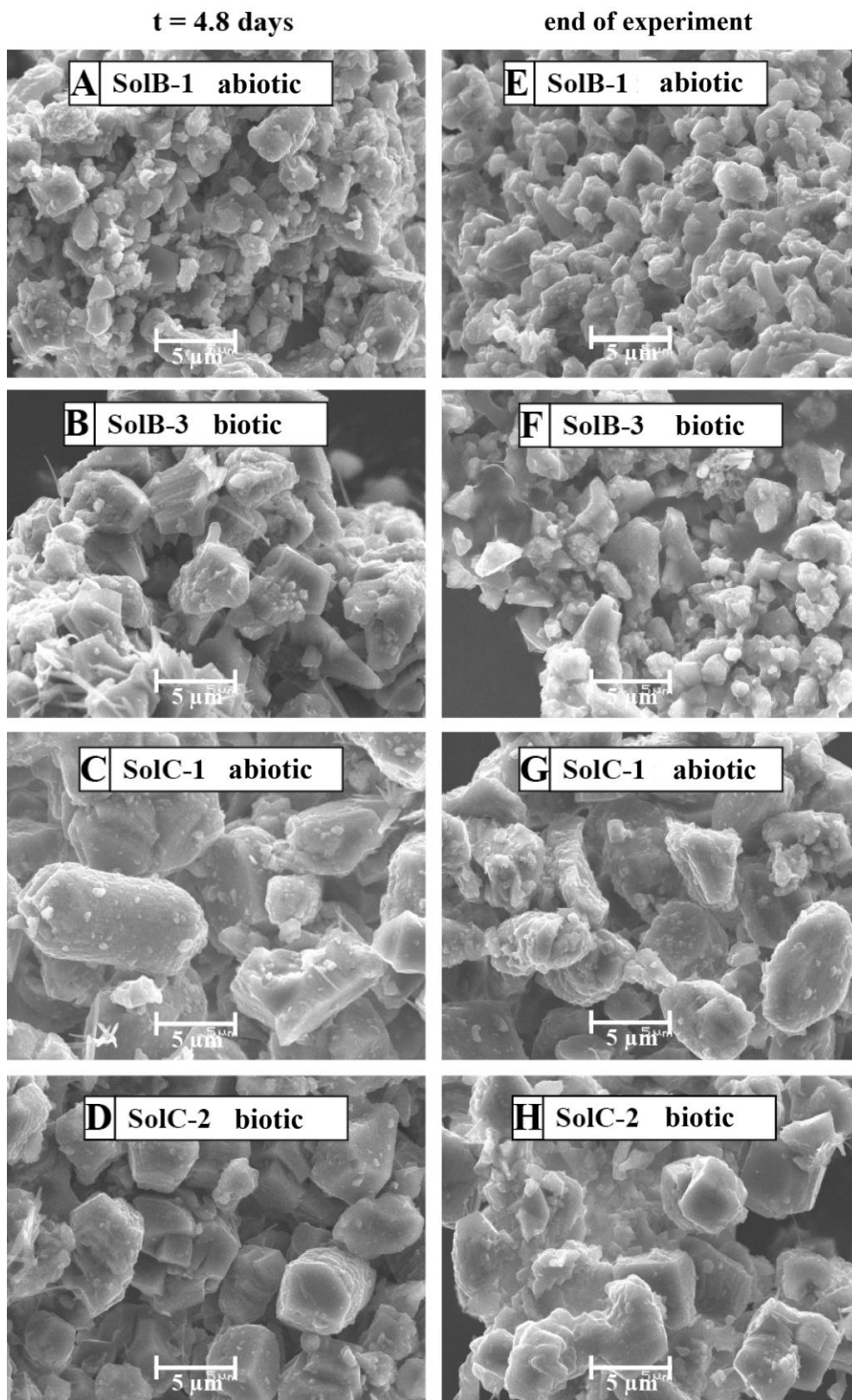


**Fig. 5.** Representative SEM images of the calcite precipitated in this study. The images on the left show calcite sampled after 4.8 days of experiments SolB-1i (A), SolB-3 (B), SolC-1i (C) and SolC-3 (D), whereas the images on the right show calcite sampled after these experiments.

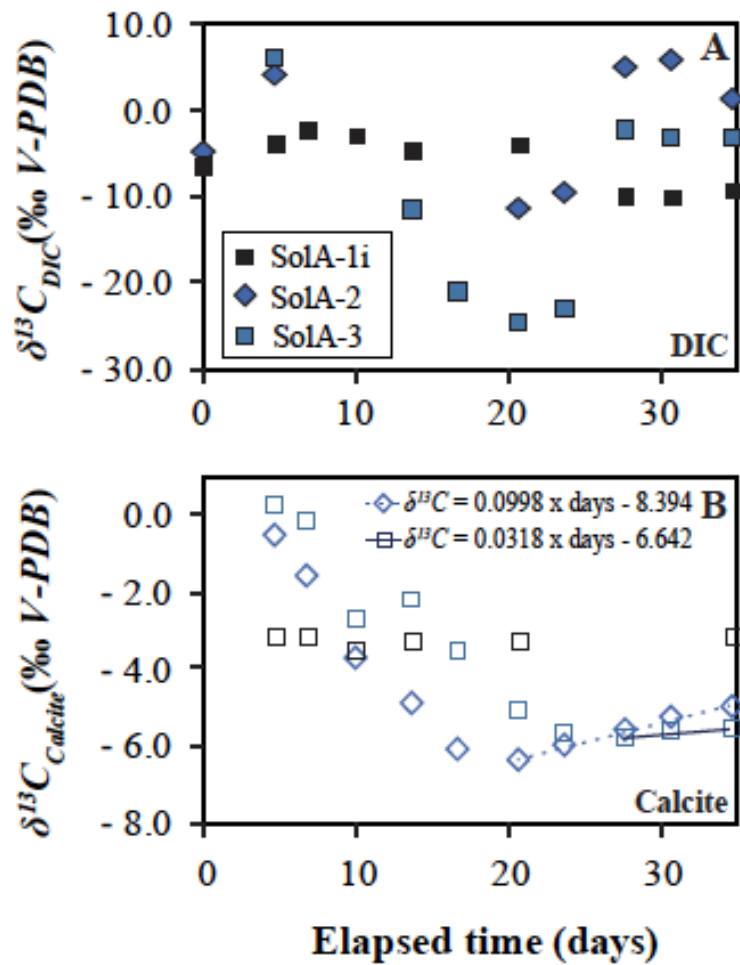


**Fig. 6.** The temporal evolution of  $\delta^{13}C_{DIC}$  (A) and  $\delta^{13}C_{Calcite}$  (B) during experimental series SolA. The analytical uncertainties ( $1\sigma$ ) of the carbon isotope measurement are  $0.1\text{‰}$  and are smaller than the symbol size. The black squares, blue diamonds and blue squares in A correspond to measured  $\delta^{13}C_{DIC}$  during experiments SolA-1i, SolA-2 and SolA-3, respectively, whereas the black outlined squares, blue outlined diamonds and the blue outline squares in B correspond to measured  $\delta^{13}C_{Calcite}$  during experiments SolA-1i, SolA-2 and SolA-3, respectively. Lines in (B) are linear regressions of the  $\delta^{13}C_{Calcite}$  evolution after completion of calcite precipitation. Equations shown in Fig. 6B correspond to the regression of the final five measured  $\delta^{13}C_{Calcite}$  of experiment SolA-2 (dashed line) and the final 3 measured  $\delta^{13}C_{Calcite}$  of experiment SolA-3 (solid line) – see text.

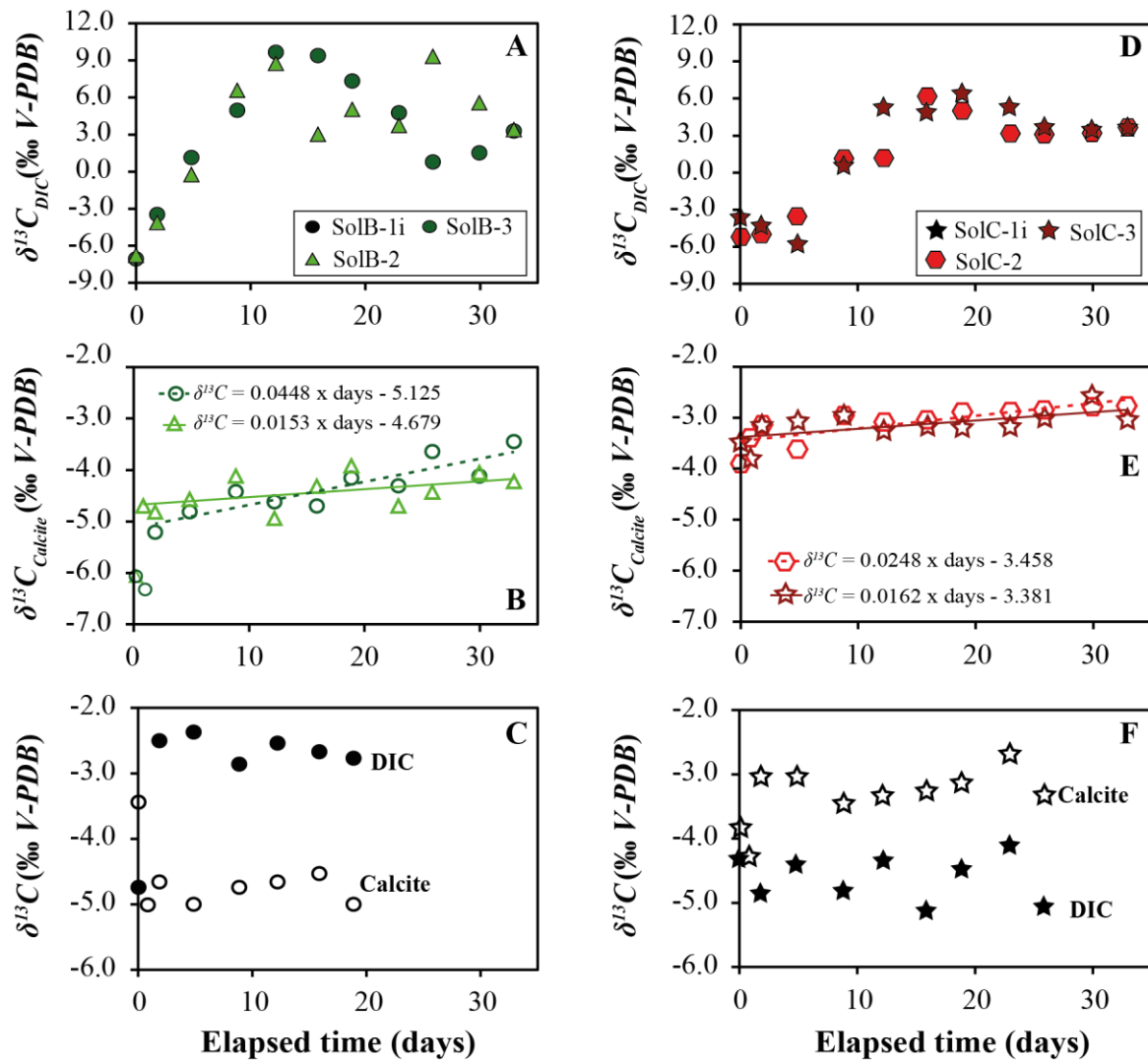


**Fig. 7.** The temporal evolution of fluid and mineral carbon isotope compositions during experimental series SolB and SolC. A)  $\delta^{13}C_{DIC}$  versus time for experiments SolB-2 and SolB-3, B)  $\delta^{13}C_{Calcite}$  versus time for experiments SolB-2 and SolB-3 C)  $\delta^{13}C_{DIC}$  and  $\delta^{13}C_{Calcite}$  versus time for experiment SolB-1i, D)  $\delta^{13}C_{DIC}$  versus time for experiments SolC-2 and SolC-3, E)  $\delta^{13}C_{Calcite}$  versus time for experiments SolC-2 and SolC-3 F)  $\delta^{13}C_{DIC}$  and  $\delta^{13}C_{Calcite}$  versus time for experiment SolC-1i. As indicated in plots A and D, values for experiments SolB-1i, SolB-2, SolB-3, SolC-1i, SolC-2 and SolC-3 are shown as black circles, green triangles, green circles, black stars, red hexagons, and red stars, respectively. Note in these plots,  $\delta^{13}C_{DIC}$  values are shown as filled symbols whereas  $\delta^{13}C_{Calcite}$  values are shown as open symbols. The analytical uncertainties ( $1\sigma$ ) of the measurement are  $0.1\text{‰}$  and are smaller than the symbol size. The lines in (B) and (E) are linear regressions of the temporal  $\delta^{13}C_{Calcite}$  evolution after completion of calcite precipitation. This regression was performed considering all measured  $\delta^{13}C_{Calcite}$  in each experiment after at least 99% of the initial aqueous calcium had precipitated. Corresponding equations are provided in Fig. (B) for experiments SolB-2 (solid line) and SolB-3 (dashed line) and in Fig. (E) for experiments SolC-2 (dashed line) and SolC-3 (solid line) – see text.

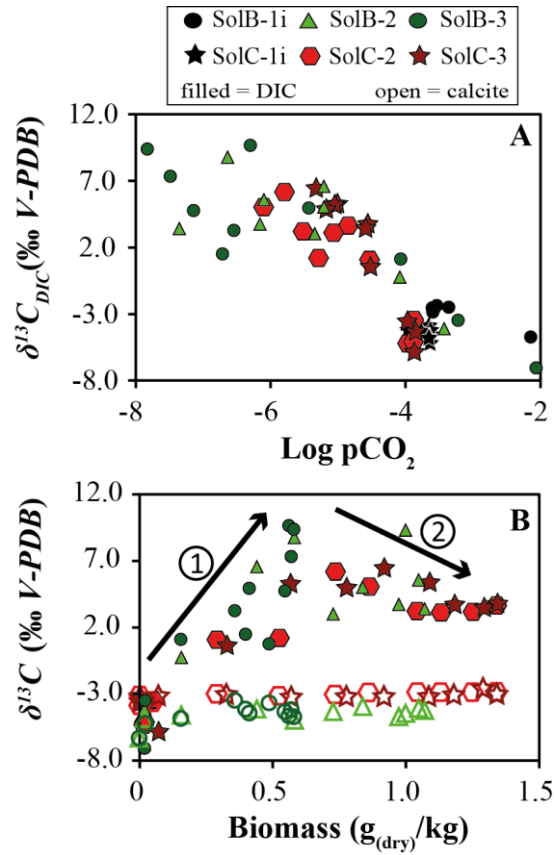


**Fig. 8.** Plot of  $\delta^{13}\text{C}_{\text{DIC}}$  as a function of  $\text{pCO}_2$  in all experiments of series SolB and SolC (A) and of  $\delta^{13}\text{C}_{\text{DIC}}$  and  $\delta^{13}\text{C}_{\text{Calcite}}$  as a function of biomass concentration in biotic experiments SolB-2, SolB-3, SolC-2 and SolC-3 (B). Arrow (1) highlights the  $\delta^{13}\text{C}_{\text{DIC}}$  increase resulting from photosynthesis which preferentially consumes  $^{12}\text{C}$  creating a liquid more enriched in  $^{13}\text{C}$ . Arrow (2) highlights the decrease in  $\delta^{13}\text{C}_{\text{DIC}}$  resulting from cell death and decomposition - see text. The symbols are identified above the figure.

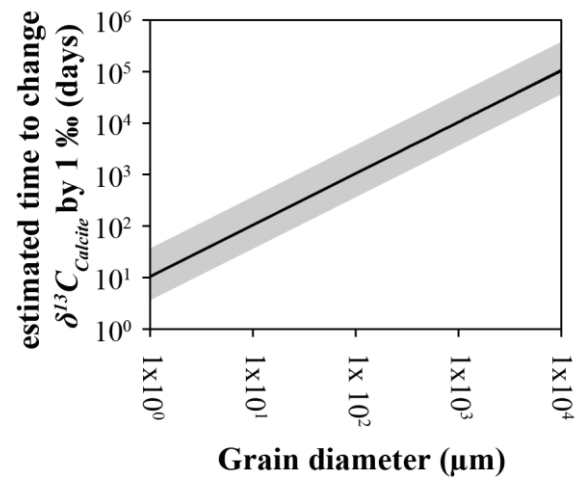


**Fig. 9.** Estimated time required to change the  $\delta^{13}\text{C}_{\text{Calcite}}$  of a calcite grain by 1‰ as a function of grain diameter. Calculations are based on the median carbon isotope exchange rates obtained in this study and assuming the calcite grains are continuously strongly out of isotope equilibrium. The grey area represents the uncertainty of the calculation, given by the variation of the obtained rates.

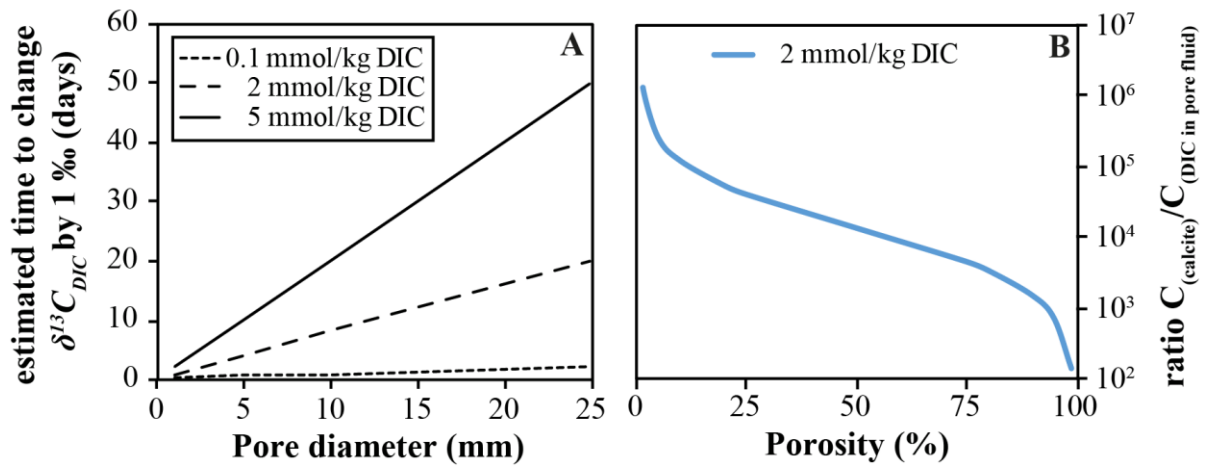


**Fig. 10. A.** Estimated time required to change the  $\delta^{13}C_{DIC}$  of porewater in a limestone by 1‰ as a function of the pore diameter, which defines the reactive surface area as well as the total mass of aqueous carbon at a defined DIC concentration in the pore fluid. The three lines correspond to the pore water DIC concentrations defined in the plot. Calculations are based on the median on carbon isotope exchange rates obtained in this study and assuming the fluid is continuously and substantially out of isotope equilibrium with the co-existing calcite (see text). The uncertainty, defined by the variation of the obtained rates, is approximately one order of magnitude. **B:** atomic ratio of carbon in calcite relative to that in a fluid phase having a dissolved inorganic carbon concentration of 2 mmol/kg within a pure limestone as a function of the rock porosity. The curve in this plot is based on the assumption that the pores are 100% water filled. The calculation shows that carbon is predominant present in the solid phase even at high porosities.

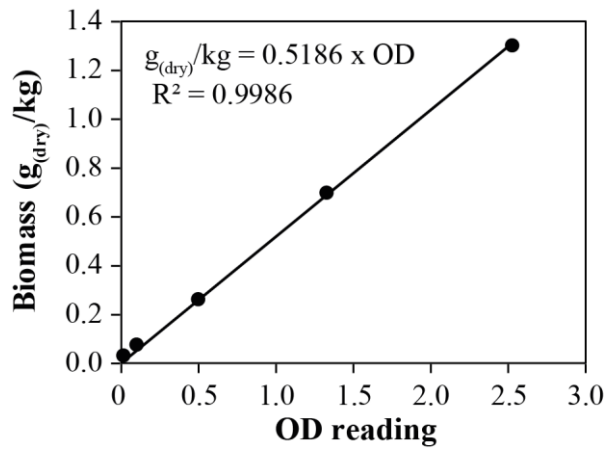


**Fig. A 1.** Optical density (OD) versus biomass (g<sub>(dry)</sub>/kg) calibration curve for determination of biomass concentrations in suspension samples.

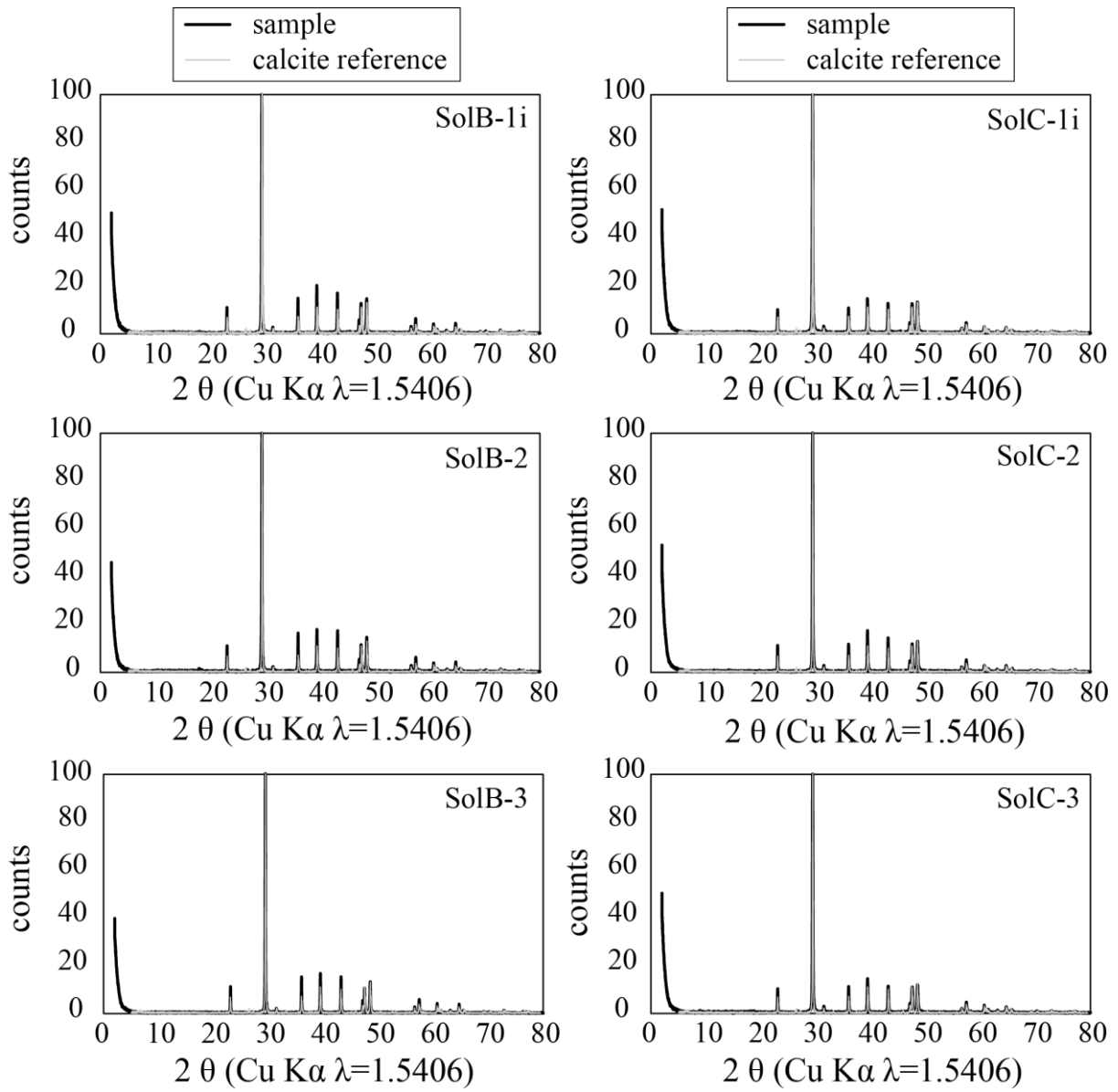


**Fig. A 2.** XRD patterns of carbonates precipitated during experiments SolB and SolC. Black lines are the samples, grey lines show the calcite reference pattern.

**Table A1.** Measured biomass concentration, pH, Ca concentration, dissolved inorganic carbon (DIC), alkalinity, C isotope composition of fluid and solid phase as well as the volume of aqueous fluid and the mass of calcite in present in the reactor for all samples examined in this study. Note that alkalinity was not measured in experiment SolA due to low carbon concentrations. Moles of calcite were calculated from the decrease in Ca concentration and the volume of fluid in the reactor. The  $\delta^{13}\text{C}_{\text{Calcite}}$  values used for the calculation of carbon isotope exchange rates are shown underlined and in bold, italic font.

ID	Time elapsed (days)	Biomass conc. (g <sub>(dry)</sub> /kg)	pH	Ca (mmol/kg)	DIC (mmol/kg)	Alkalinity (mmol/kg)	Fluid in reactor (g)	Calcite in reactor (mmol)	$\delta^{13}\text{C}_{\text{Calcite}}$ (‰ V-PDB)	$\delta^{13}\text{C}_{\text{DIC}}$ (‰ V-PDB)
SolA-Ii - 0	0.0			8.64			900			
SolA-Ii - 1	0.0		8.31	8.25	9.05		894	0.34		-6.08
SolA-Ii - 2	2.8		8.62	4.97			844	3.09		
SolA-Ii - 3	4.7		8.64	5.00	3.16		838	3.05	-3.15	-3.66
SolA-Ii - 4	6.8		8.61	4.96	3.13		788	2.90	-3.15	-2.08
SolA-Ii - 5	10.0		8.54	4.96	3.14		738	2.71	-3.53	-2.71
SolA-Ii - 6	11.7		8.65	4.89			688	2.58		
SolA-Ii - 7	13.7		8.64	5.11	3.14		682	2.40	-3.25	-4.42
SolA-Ii - 8	16.7		8.56	5.10	3.13		632	2.23		
SolA-Ii - 9	18.7		8.67	5.09			582	2.06		
SolA-Ii - 10	20.7		8.64	5.14	3.17		573	2.00	-3.26	-3.77
SolA-Ii - 11	23.7		8.65	4.94	3.11		523	1.93		
SolA-Ii - 12	25.7		8.68	4.99			473	1.72		
SolA-Ii - 13	27.7		8.59	5.04	3.16		467	1.68		-9.76
SolA-Ii - 14	30.7		8.66	5.18	3.21		417	1.44		-9.81
SolA-Ii - 15	32.7		8.63				367			
SolA-Ii - 16	34.7		8.62	5.20	3.23		359	1.23	-3.16	-9.01
SolA-2 - 0	0.0			8.60			900			
SolA-2 - 1	0.0	0.016	8.32	8.19	9.10		894	0.37	-13.61	-4.64
SolA-2 - 2	2.8	0.004	8.69	4.50			844	3.46		
SolA-2 - 3	4.7	0.076	9.49	3.35	0.94		838	4.40	-0.53	4.25
SolA-2 - 4	6.8	0.215	10.49	2.82	0.36		788	4.55	-1.59	
SolA-2 - 5	10.0	0.445	10.60	2.18	0.28		738	4.73	-3.73	
SolA-2 - 6	11.7	0.582	10.76	1.88			688	4.62		
SolA-2 - 7	13.7	0.740	10.62	1.51	0.37		682	4.83	-4.91	
SolA-2 - 8	16.7	0.927	10.35	0.89	0.42		632	4.87	-6.11	
SolA-2 - 9	18.7	1.073	10.28	0.49			582	4.72		
SolA-2 - 10	20.7	1.190	10.02	0.25	0.71		573	4.78	-6.39	-11.21
SolA-2 - 11	23.7	1.337	9.93	0.12	1.47		523	4.43	<b><u>-6</u></b>	-9.37
SolA-2 - 12	25.7	1.474	9.32	0.17			473	3.99		
SolA-2 - 13	27.7	1.672	9.47	0.10	2.97		467	3.97	<b><u>-5.6</u></b>	5.14
SolA-2 - 14	30.7	1.774	9.30	0.12	3.57		417	3.53	<b><u>-5.27</u></b>	5.98
SolA-2 - 15	32.7	1.811	9.20	0.10			367			
SolA-2 - 16	34.7	1.852	9.09	0.17	3.91		359	3.02	<b><u>-5</u></b>	1.46
SolA-3 - 0	0.0			8.54			900			
SolA-3 - 1	0.0	0.015	8.25	8.26	9.04		894	0.25	-9.1	-6.37
SolA-3 - 2	2.8	0.001	8.71	4.74			844	3.20		
SolA-3 - 3	4.7	0.053	9.42	3.28	0.72		838	4.40	0.25	6.25
SolA-3 - 4	6.8	0.194	10.77	3.00	0.23		788	4.36	-0.14	
SolA-3 - 5	10.0	0.376	10.74	2.40	0.24		738	4.53	-2.71	
SolA-3 - 6	11.7	0.480	10.94	2.16			688	4.38		
SolA-3 - 7	13.7	0.585	10.80	1.78	0.54		682	4.60	-2.21	-11.32
SolA-3 - 8	16.7	0.732	10.51	1.11	0.57		632	4.69	-3.55	-20.85
SolA-3 - 9	18.7	0.797	10.23	0.81			582	4.50		
SolA-3 - 10	20.7	0.939	10.38	0.53	0.50		573	4.58	-5.08	-24.38
SolA-3 - 11	23.7	1.100	10.87	0.31	0.62		523	4.30	-5.69	-22.82
SolA-3 - 12	25.7	1.248	9.85	0.11			473	3.98		
SolA-3 - 13	27.7	1.411	10.00	0.06	1.69		467	3.95	<b><u>-5.79</u></b>	-2.09
SolA-3 - 14	30.7	1.612	10.08	0.05	2.31		417	3.53	<b><u>-5.62</u></b>	-3.11
SolA-3 - 15	32.7	1.703	9.68				367			
SolA-3 - 16	34.7	1.755	10.01	0.06	2.82		359	3.04	<b><u>-5.56</u></b>	-3.01
SolB-Ii - 1	0.0		8.59	8.50	47.60	51.53	897	0.00		
SolB-Ii - 2	0.0	0.003	8.31	8.23	29.50	33.23	847	0.23	-3.44	-4.74
SolB-Ii - 3	0.8		9.20	0.15		32.39	837	6.99	-5.01	
SolB-Ii - 4	1.9	0.005	9.41	0.07	28.42	32.14	787	6.63	-4.66	-2.5

ID	Time elapsed (days)	Biomass conc. (g <sub>(dry)</sub> /kg)	pH	Ca (mmol/kg)	DIC (mmol/kg)	Alkalinity (mmol/kg)	Fluid in reactor (g)	Calcite in reactor (mmol)	$\delta^{13}\text{C}_{\text{Calcite}}$ (‰ V-PDB)	$\delta^{13}\text{C}_{\text{DIC}}$ (‰ V-PDB)
SolB-1i - 5	4.8	0.011	9.54	0.05	27.49	32.12	737	6.23	-5	-2.37
SolB-1i - 6	6.8	0.005	9.53				734			
SolB-1i - 7	8.8	0.002	9.58	0.03	28.56	32.34	684	5.79	-4.74	-2.86
SolB-1i - 8	12.2	0.008	9.59	0.03	28.64	32.37	634	5.37	-4.66	-2.54
SolB-1i - 9	14.1	0.002	9.56				631			
SolB-1i - 10	15.9	0.013	9.58	0.03	27.31	32.51	581	4.92	-4.53	-2.67
SolB-1i - 11	18.9	0.015	9.58	0.03	27.89	32.56	531	4.50	-5	-2.77
SolB-2 - 1	0.0	0.017	8.59	8.50	47.60	51.53	897	0.00		
SolB-2 - 2	0.0	0.018	8.20	7.98	32.37	35.60	847	0.44	-6.3	-6.78
SolB-2 - 3	0.8		9.13	0.13		32.44	837	7.01	-4.7	
SolB-2 - 4	1.9	0.018	9.46	0.06	28.96	32.37	787	6.64	<u>-4.82</u>	-4.11
SolB-2 - 5	4.8	0.157	9.91	0.04	26.19	33.34	737	6.24	<u>-4.57</u>	-0.25
SolB-2 - 6	6.8	0.302	10.22				734			
SolB-2 - 7	8.8	0.440	10.55	0.02	22.36	33.26	684	5.80	<u>-4.12</u>	6.58
SolB-2 - 8	12.2	0.580	11.29	0.02	21.92	35.61	634	5.37	<u>-4.94</u>	8.76
SolB-2 - 9	14.1	0.652	10.77				631			
SolB-2 - 10	15.9	0.727	10.64	0.02	23.99	36.25	581	4.93	<u>-4.32</u>	3.01
SolB-2 - 11	18.9	0.837	10.57	0.02	24.38	36.89	531	4.50	<u>-3.92</u>	5.02
SolB-2 - 12	20.9	0.918	10.71				528			
SolB-2 - 13	22.9	0.973	11.06	0.02	22.46	37.51	478	4.05	<u>-4.7</u>	3.74
SolB-2 - 14	25.9	0.999	11.60	0.02	20.55		428	3.63	<u>-4.43</u>	9.32
SolB-2 - 15	27.9	1.017	11.17			37.73	425			
SolB-2 - 16	29.9	1.047	11.03	0.02	24.32	38.01	375	3.18	<u>-4.05</u>	5.57
SolB-2 - 17	32.9	1.070	11.65	0.02	21.56	38.13	325	2.76	<u>-4.23</u>	3.39
SolB-3 - 1	0.0	0.017	8.58	8.50	47.60	51.53	897	0.00		
SolB-3 - 2	0.0	0.018	8.25	7.88	31.74	34.46	847	0.53	-6.3	-7.06
SolB-3 - 3	0.8		8.84	0.21		33.34	837	6.94	-6.56	
SolB-3 - 4	1.9	0.020	9.31	0.07	29.71	33.28	787	6.63	<u>-5.21</u>	-3.48
SolB-3 - 5	4.8	0.154	9.91	0.04	29.83	33.77	737	6.24	<u>-4.81</u>	1.13
SolB-3 - 6	6.8	0.281	10.30				734			
SolB-3 - 7	8.8	0.411	10.68	0.02	20.49	35.22	684	5.80	<u>-4.42</u>	4.95
SolB-3 - 8	12.2	0.561	11.12	0.03	19.80	35.99	634	5.37	<u>-4.62</u>	9.65
SolB-3 - 9	14.1	0.582	11.72				631			
SolB-3 - 10	15.9	0.579	11.85	0.02	27.72	36.00	581	4.92	<u>-4.7</u>	9.39
SolB-3 - 11	18.9	0.569	11.70	0.02	21.95	36.02	531	4.50	<u>-4.16</u>	7.34
SolB-3 - 12	20.9	0.561	11.68				528			
SolB-3 - 13	22.9	0.545	11.54	0.02	21.11	36.07	478	4.05	<u>-4.31</u>	4.76
SolB-3 - 14	25.9	0.486	11.49	0.03	18.54		428	3.63	<u>-3.64</u>	0.78
SolB-3 - 15	27.9	0.439	11.51			36.05	425			
SolB-3 - 16	29.9	0.397	11.33	0.03	20.99	35.94	375	3.18	<u>-4.12</u>	1.51
SolB-3 - 17	32.9	0.357	11.25	0.03	23.64	36.00	325	2.75	<u>-3.45</u>	3.28
SolC-1i - 1	0.0		10.14	8.50	48.94	71.61	897	0.00		
SolC-1i - 2	0.0	0.004	9.94	0.82	41.71	56.19	847	6.50	-3.84	-4.31
SolC-1i - 3	0.8		9.98	0.05		56.16	837	7.07	-4.26	
SolC-1i - 4	1.9	0.004	9.92	0.04	44.45	56.07	787	6.66	-3.04	-4.82
SolC-1i - 5	4.8	0.006	9.83	0.04	45.43	56.31	737	6.23	-3.04	-4.39
SolC-1i - 6	6.8	0.003	9.79				734			
SolC-1i - 7	8.8	0.007	9.78	0.03	46.66	57.02	684	5.79	-3.44	-4.81
SolC-1i - 8	12.2	0.012	9.77	0.03	47.77	56.78	634	5.37	-3.32	-4.34
SolC-1i - 9	14.1	0.008	9.75				631			
SolC-1i - 10	15.9	0.014	9.76	0.02	45.97	56.59	581	4.92	-3.25	-5.12
SolC-1i - 11	18.9	0.015	9.75	0.02	49.89	57.12	531	4.50	-3.13	-4.46
SolC-1i - 12	20.9	0.004	9.77				528			
SolC-1i - 13	22.9	0.020	9.76	0.02	46.28	57.65	478	4.05	-2.67	-4.09
SolC-1i - 14	25.9	0.018	9.80	0.02	45.86		428	3.60	-3.30	-5.04
SolC-2 - 1	0.0	0.017	10.14	8.50	48.94	71.61	897	0.00		
SolC-2 - 2	0.0	0.015	9.95	0.08	43.06	57.12	847	7.13	-3.89	-5.23
SolC-2 - 3	0.8		9.98	0.04		57.18	837	7.08	<u>-3.38</u>	
SolC-2 - 4	1.9	0.017	9.92	0.04	49.13	57.29	787	6.66	<u>-3.13</u>	-5.07
SolC-2 - 5	4.8	0.048	9.91	0.04	44.40	57.52	737	6.24	<u>-3.61</u>	-3.48
SolC-2 - 6	6.8	0.138	10.07				734			
SolC-2 - 7	8.8	0.289	10.29	0.03	42.07	59.27	684	5.80	<u>-2.94</u>	1.08
SolC-2 - 8	12.2	0.525	10.71	0.02	37.15	61.29	634	5.37	<u>-3.08</u>	1.21
SolC-2 - 9	14.1	0.645	10.86				631			
SolC-2 - 10	15.9	0.734	10.97	0.02	38.36	62.35	581	4.93	<u>-3.03</u>	6.2

ID	Time elapsed (days)	Biomass conc. (g <sub>(dry)</sub> /kg)	pH	Ca (mmol/kg)	DIC (mmol/kg)	Alkalinity (mmol/kg)	Fluid in reactor (g)	Calcite in reactor (mmol)	$\delta^{13}\text{C}_{\text{Calcite}}$ (‰ V-PDB)	$\delta^{13}\text{C}_{\text{DIC}}$ (‰ V-PDB)
SolC-2 - 11	18.9	0.860	11.12	0.02	35.30	63.20	531	4.50	<u>-2.86</u>	5.05
SolC-2 - 12	20.9	0.952	10.92				528			
SolC-2 - 13	22.9	1.041	10.83	0.02	37.57	64.55	478	4.06	<u>-2.86</u>	3.2
SolC-2 - 14	25.9	1.130	10.68	0.02	38.70		428	3.63	<u>-2.82</u>	3.13
SolC-2 - 15	27.9	1.201	10.70			65.58	425			
SolC-2 - 16	29.9	1.251	10.60	0.02	44.22	67.02	375	3.18	<u>-2.79</u>	3.16
SolC-2 - 17	32.9	1.339	10.50	0.03	43.28	67.93	325	2.75	<u>-2.77</u>	3.64
SolC-3 - 1	0.0	0.017	10.13	8.50	48.94	71.61	897	0.00		
SolC-3 - 2	0.0	0.017	9.96	0.27	44.82	56.68	847	6.97	-3.47	-3.51
SolC-3 - 3	0.8		9.95	0.06		56.86	837	7.07	<u>-3.79</u>	
SolC-3 - 4	1.9	0.019	9.89	0.04	48.76	56.75	787	6.66	<u>-3.14</u>	-4.26
SolC-3 - 5	4.8	0.069	9.90	0.04	46.59	57.21	737	6.24	<u>-3.06</u>	-5.81
SolC-3 - 6	6.8	0.171	10.05				734			
SolC-3 - 7	8.8	0.326	10.28	0.03	42.24	59.09	684	5.79	<u>-2.94</u>	0.59
SolC-3 - 8	12.2	0.566	10.57	0.03	36.29	60.67	634	5.37	<u>-3.23</u>	5.27
SolC-3 - 9	14.1	0.683	10.62				631			
SolC-3 - 10	15.9	0.775	10.65	0.03	40.25	62.22	581	4.92	<u>-3.17</u>	4.92
SolC-3 - 11	18.9	0.918	10.73	0.03	41.07	63.45	531	4.50	<u>-3.18</u>	6.46
SolC-3 - 12	20.9	1.022	10.63				528			
SolC-3 - 13	22.9	1.087	10.57	0.03	44.56	64.95	478	4.05	<u>-3.16</u>	5.35
SolC-3 - 14	25.9	1.180	10.50	0.06	43.89		428	3.61	<u>-2.99</u>	3.68
SolC-3 - 15	27.9	1.242	10.44			66.28	425			
SolC-3 - 16	29.9	1.290	10.35	0.03	47.24	67.80	375	3.18	<u>-2.57</u>	3.51
SolC-3 - 17	32.9	1.342	10.34	0.04	47.06	68.57	325	2.75	<u>-3.03</u>	3.75